

AD-A231 598

May 1990

THESIS/~~DISSERTATION~~

A Search for Episodic Increases in Upper Atmospheric
Water Vapor as Evidence of An Extraterrestrial Source

Michael F. Bonadonna

AFIT Student Attending: Pennsylvania State University

AFIT/CI/CIA-90-128

AFIT/CI

Wright-Patterson AFB OH 45433-6583

Approved for Public Release IAW 190-1
Distributed Unlimited
ERNEST A. HAYGOOD, 1st Lt, USAF
Executive Officer

DTIC
ELECTE
FEB 07 1991
S B D

The Pennsylvania State University

The Graduate School

Department of Meteorology

A SEARCH FOR EPISODIC INCREASES IN UPPER ATMOSPHERIC
WATER VAPOR AS EVIDENCE OF AN EXTRATERRESTRIAL SOURCE

A Thesis in

Meteorology

by

Michael F. Bonadonna

Submitted in Partial Fulfillment
of the Requirements
for the Degree of

Master of Science

May 1990

91 2 06 100

I grant The Pennsylvania State University the nonexclusive right to use this work for the University's own purposes and to make single copies of the work available to the public on a not-for-profit basis if copies are not otherwise available.

Michael F. Bonadonna

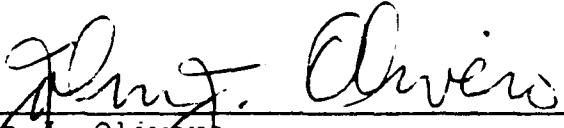
Michael F. Bonadonna



Accession For	
NTIS GRA&I	<input checked="checked" type="checkbox"/>
DTIC TAB	<input type="checkbox"/>
Unannounced	<input type="checkbox"/>
Justification	
By	
Distribution/	
Availability Codes	
and/or	
Special	
A-1	

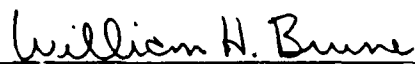
We approve the thesis of Michael F. Bonadonna.

Date of Signature




John J. Olivero
Professor of Meteorology
Thesis Advisor

21 Feb. '90



William H. Brune
Associate Professor of Meteorology

22 February, 1990



William M. Frank
Associate Professor of Meteorology
Head of the Department of Meteorology

22 Feb 1990

ABSTRACT

This study examines the short-term variability of upper atmospheric water vapor with the intent of examining a proposed extraterrestrial water vapor source. This source would be provided by an influx of the small (12 m in diameter) comets described by Frank et al. (1986b). A ground-based microwave (22.235 GHz) radiometer located at Penn State has been measuring the thermal emission of upper atmospheric water vapor since 1984. Over 22,000 20-minute brightness temperature spectra from the period of November 1984 through December 1988 were analyzed for statistically significant, transient increases of the amounts of water vapor. This signature could indicate the presence of the cometary water vapor source. Individual 20-minute spectra were compared to the local 12-hour mean and variance spectra in a search for this excess signal signature or event.

The analysis yielded 111 significant events which could have been caused by the cometary water vapor. The rate of detection (2.9 days between events) compares favorably with what could be expected from the small comet theory (1.8 days/event). This result is also comparable to the 4.1 days/event obtained by Adams (1988) using a small subset of this data base. After exploring alternate explanations for the observed phenomena, it is concluded that these results support the existence of the small comet hypothesis.

TABLE OF CONTENTS

	Page
LIST OF TABLES	vi
LIST OF FIGURES	vii
ACKNOWLEDGEMENTS	viii
Chapter	
1 INTRODUCTION	1
1.1 Background	1
1.2 Statement of the problem	3
1.3 Outline of thesis	5
2 THE SMALL COMET HYPOTHESIS	6
2.1 Arguments opposing the small comet hypothesis	8
2.2 Arguments having implication for the middle and upper atmosphere	10
3 WATER VAPOR IN THE MESOSPHERE	13
3.1 Current knowledge of mesospheric water vapor	13
3.2 The impact of small comets on mesospheric models	19
3.3 Methods of observing mesospheric water vapor	20
3.4 The Penn State microwave radiometer...	21
4 THEORETICAL CONSIDERATIONS	29
4.1 Radiative transfer equation	29
4.2 Spectral line broadening	32
4.3 Inversion of spectral data	33
5 EXPERIMENTAL PROCEDURES	37
5.1 Data preparation and handling	37
5.2 Analysis procedures	38
5.3 Unusable data identification	40
5.4 Search procedures	41

6	STATISTICAL CONSIDERATIONS	44
6.1	Folding and integration	44
6.2	The Z and normality tests	46
6.3	Event detection	49
7	RESULTS AND DISCUSSION	52
7.1	The data	52
7.2	The detected events	54
7.2.1	Low resolution time line	54
7.2.2	High resolution time line	57
7.2.3	Data statistics	66
7.2.4	Trend analysis	69
7.3	Selected case studies	72
7.4	Examination of spectral wings	78
7.5	Rocket water release experiment	81
7.6	Possible causes of events	83
8	SUMMARY, CONCLUSIONS, AND RECOMMENDATIONS FOR FUTURE WORK	89
8.1.	Summary	89
8.2.	Conclusions	90
8.3.	Recommendations for future work	91
	BIBLIOGRAPHY	94

LIST OF TABLES

	Page
7.1. Period of Record	53
7.2. Summary of Detected Events	55
7.3. Summary of Event Statistics	67
7.4. Summary of Spectral Wing Analysis	80

LIST OF FIGURES

	Page
3.1. Vertical and meridional distribution of water vapor. (mean values for December)	14
3.2. Season variations in mesospheric water vapor	16
3.3. Penn State microwave radiometer block diagram	25
6.1. Results of the the test for normal distribution including the linear regression equation	48
7.1. Low resolution event time line	56
7.2. High resolution event time line	58
7.3. Case study of a near threshold P-value event spectrum	73
7.4. Case study of an extremely small P-value event spectrum	74
7.5. Case study of a typical event spectrum	76
7.6. Vertical water vapor mixing ratio profiles for the event at 0320L on 18 March 1986	77

ACKNOWLEDGEMENTS

I would like to thank Mr. Robert Divany for his diligent assistance during the software development and data transfer phase of the project. His contribution is reflected in each bit of data.

Special thanks are due to Dr. C. Russell Philbrick with whom I shared many enlightening discussions and whose vision of our future in science is truly inspirational.

I extend my sincere gratitude to Dr. Charles L. Croskey, whose dedication to the design and operation of the equipment as well as our frequent consultations helped keep the project on track.

For the helpful comments of my thesis reader, Dr. William H. Brune, I am very grateful.

My deepest thanks go to my thesis advisor, Dr. John J. Olivero, for his patience, encouragement, and consistently sound guidance during the course of this research.

Finally, I thank my wife, Eve, for her candid editorial assistance, typing and graphics support, and being there when I needed her most.

Chapter 1

INTRODUCTION

1.1 Background

In 1986 a hypothesis was proposed that the earth's atmosphere is being bombarded by small (water-ice) comet-like bodies at a rate of 20 collisions per minute (Frank et al., 1986a). If this were true 10^{12} Kg/year of water vapor would be deposited into the upper atmosphere (that part of the atmosphere above the tropopause) by these small comets. This addition of water vapor would have profound implications on the photochemistry and ion chemistry of the upper atmosphere.

Although water vapor is a trace constituent above the tropopause it plays a major role in the photochemistry of ozone (Hunt 1966). Ozone concentrations in the mesosphere are theoretically linked to water vapor concentrations since water vapor is the primary source of odd hydrogen, which controls ozone destruction at these altitudes (Allen et al. 1981). Atoms and molecules which are ionized in the middle atmosphere by solar UV radiation produce free electrons and ions to which water molecules may become electrostatically bonded thus producing cluster ions. The number of free electrons could be reduced since the recombination rate for molecular ions is less than that of cluster ions. This decrease in electron density could cause significant

weakening of the ionosphere thus altering radio wave propagation which could disrupt normal radio communications. Beyond this, being that water is a strong absorber and emitter of IR radiation, the radiative balance of the earth system could be altered. At the very least, our understanding of the maintenance of these balances would have to be revised to account for this new water vapor source.

Several research groups have investigated various aspects of the small comet hypothesis. Their results have provided evidence which both supports and refutes the original theory. The search for Frank's small comets was also carried out here at Penn State by Dennis Adams (1988). Adams' findings were astounding. Using microwave radiometry techniques he looked for short-term variability in mesospheric water vapor which he believed was a signature of small comet penetration into the atmosphere. He found at least four cases in which anomalous water vapor was apparently detected during a two-month period. He reasoned that the additional water vapor was most likely of extraterrestrial origin and therefore consistent with the Frank small comet theory. This thesis is a logical extension of his work -- to increase the data set analyzed.

Observations of the water vapor profile of the stratosphere have been conducted since the 1950's. These early measurements were obtained using in situ methods

(aircraft, balloons and rockets). In the 1970's, technological advances made possible the use of remote sensing techniques for obtaining water vapor profiles of the mesosphere and lower thermosphere. Since that time, more capable systems have been designed for this purpose. Ground-based microwave radiometers are now able to retrieve information regarding water vapor concentrations though altitudes between 55 and 80 kilometers on a continual basis. The results of several years of observations show the upper mesosphere is quite dry (Tsou 1986, and Bevilacqua et al., 1989a).

If the small comet theory is true, large amounts of water vapor are being injected in isolated, short bursts into localized areas of the upper atmosphere. This water vapor should be detectable by a ground based microwave radiometer if the water vapor has sufficient residence time within the radiometer's field of view. Over short time periods, the radiometer outputs tend to be noise dominated; therefore, in order to examine these short time periods for the presence of water vapor introduced by small icy comets, a statistical approach must be adopted.

1.2 Statement of the problem

Adams manually examined approximately 1400 20-minute observations to uncover 4 possible detections of water vapor

from small comets. Now, several years of data are available and could be used to search for possible "events" by computer automated analysis. This search can also be enhanced by the use of statistical analysis to suggest the confidence level of our results and help separate such "events" from the natural geophysical variability and instrument noise.

Water vapor from a small comet entering the earth's atmosphere would remain in the radiometer's beam from a few seconds to a few minutes. A large amount of water vapor should be detectable within the shortest time period observation recorded by the radiometer, the 20-minute integration. This 20-minute integration should indicate water vapor concentrations that greatly exceed those of the 12-hour integration to which it contributes. Once an observation is identified as an "event" it is compared to its neighboring observations to determine if it is an isolated event in time. Finally, the frequency distribution of the detected events will be compared to that of which would be expected from the small comet theory to determine if the detected events could be caused by the small comet impacts.

1.3 Outline of thesis

The remainder of this thesis conforms to the following outline. The second chapter describes the small comet theory as well as arguments which support and refute it. In chapter 3, methods of observing mesospheric water vapor are discussed as well as our current understanding of its role in the middle atmosphere. In chapter 4, we review the basic elements of microwave radiometry as they impact on the present study. Chapter 5 outlines the experimental procedures. Chapter 6 clarifies the statistical treatment of the data. Chapter 7 presents the results and discussion. Finally, the experiment is summarized, conclusions drawn and recommendations for future work are given in chapter 8.

Chapter 2

THE SMALL COMET HYPOTHESIS

In April 1986, the cover article of Geophysical Research Letters was entitled, "On the Influx of Small Comets into the Earth's Atmosphere" by L.A. Frank and his associates from the University of Iowa. The paper showed startling evidence, from the Dynamics Explorer-1 satellite, that the earth was being bombarded by small, icy comet-like objects at a rate of 20 per minute! This speculation was based on a series of dark spots on the earth's atomic oxygen dayglow images which later became known as "atmospheric holes." What made this statement so remarkable was Frank's calculation of the size (about 12 meters in diameter) and mass (about 10^5 Kg) of these small comets. If the cometary influx theory is correct, our understanding of the origins and distribution of water vapor throughout the atmosphere might be forced to undergo significant changes.

Several factors lead Frank et al. (1986b) to the conclusion that the atmospheric holes were of extraterrestrial origin. First, using a statistical analysis of the distribution of sightings, comparisons were made that eliminated telemetry noise, recorder error and sensor error as possible explanations for the atmospheric holes. Secondly, a significant diurnal variation in the location of the holes was observed to be similar to those

that would be expected for meteors. Finally, these atmospheric holes were noticed on limb viewing imagery above the exobase. This would not have been possible if the holes were caused by a terrestrial source (Frank et al. 1986b).

Frank and his coworkers (J.B. Sigworth and J.D. Craven) hypothesized that, based on the observations, the small comets (also known as FSC bodies) would be composed of water and trace amounts of metallic compounds in the form of a fluffy aggregate covered with a dust mantle with a tensile strength of around $.1 \text{ dyne cm}^{-2}$. The impact speed at the top of the atmosphere would have to be around 20 m/sec to explain why the small comets don't create an ionization trail upon entry to the atmosphere. Frank and his associates theorized that the comets would first be disrupted at 500 km altitude and travel downward as a spreading "cloud" of sublimated water molecules. As stated earlier the comet should have a mass and size of 10^8 gm and 12 meter diameter thus a possessing a density of $.1 \text{ gm/cm}^3$. Finally, the FSC bodies would have an influx rate of 20 per minute globally, thus depositing 10^{12} Kg/year of water into the Earth system.

Frank et al. suggested possible interpretations of the atmospheric holes. However, after exploring these possible explanations the authors believed the most plausible was that they were caused by absorption of dayglow emissions by the water vapor liberated from small comets. They also

stated that the water vapor from the FSC bodies would not penetrate the atmosphere below 125 Km as a coherent mass but that diffusion and other dynamic processes could carry the molecules to lower altitudes.

2.1 Arguments opposing the small comet hypothesis

After the publication of the paper by Frank et al., many arguments opposing the small comet theory began appearing in the technical journals. These arguments are briefly summarized below. Those that have direct implications on the middle atmosphere are discussed in greater detail. For a complete synopsis refer to Frank (1989). Objections to the Frank small comet hypothesis fall into three general categories: (1) inconsistencies of the hypothesis with other current hypotheses, (2) the presence of contradictory or lack of substantial supporting observational data, and (3) criticisms of the manner in which the data used by Frank et al. was retrieved, processed, or analyzed.

(1) Inconsistencies with other hypotheses:

- Retrograde as well as prograde orbits should be possible thus causing impact speeds to be much higher (Morris 1986).
- Additional water source would add the equivalent of two

extra oceans on Earth (Donahue 1986).

- Water should have been deposited on Venus and Mars (Donahue 1986).
- Proposed composition of the comets are implausible (Wasson & Kyte 1987).
- Low velocity and inclination of accretion is vastly different from other comets or meteors (Wasson & Kyte 1987).
- Proposed orbits suggest comets have a relatively long life and thus need larger/stronger mantles (McKay 1986).

(2) Conflict with observational data:

- Not enough iridium nor chondrites on Earth for a large influx of extraterrestrial material (Morris 1986; Wasson & Kyte 1987).
- Small comet are not detected by optical telescopes (Soter 1987)
- No small comet impacts recorded by lunar seismographs (Davis 1986).

(3) Criticism of data handling

- Atmospheric holes appear in single pixels of dayglow images thus could be data artifacts or errors (Chubb 1986).
- Hole distribution and appearance is independent of

satellite altitude thus suggesting they are instrument errors (Cragin et al. 1986)

2.2 Arguments having implications for the middle and upper atmosphere

One of the major objections to the original hypothesis, having implications on the middle and upper atmosphere, was brought to light by Donahue (1986). If 4×10^{31} water molecules per minute were being deposited into the atmosphere above the turbopause the largest water vapor concentration would be found in the lower thermosphere and the hydrogen escape flux would be increased due to the photodissociation of the cometary water molecules. These conditions are contrary to those observed.

In response to these arguments, Frank et al. (1986c), made several adjustments to their small comet theory. They suggested that initial impact velocities could be as large as 4 km/sec, at 120 km altitude, but less than 1% of the comets mass would be lost there. Most of the frictional energy would go to the deceleration of the comet, rather than to heat production. As the comet entered the atmosphere it would break up into a dense "cloud" of water molecules, slowly spreading as it traveled downwards. Frictional forces would decelerate the cloud and entrainment would keep it from losing much of its mass at high altitudes. As it moved into the denser mesosphere, it would

rapidly decelerate and dissipate leaving the majority of its water molecules in the lower mesosphere, thus alleviating the transport problems above the turbopause cited by Donahue.

According to Hanson (1986), the comet influx rate is also inconsistent with measurements of ionospheric plasmas, by several spacecraft. He assumed that the interaction of the water "cloud" with the ionosphere could be described by single particle mechanisms, eg. charge exchange and ion diffusion. Hanson looked for perturbations caused by these interactions, found no evidence of them, and concluded that the small comet theory must be erroneous.

Frank et al. (1986d), suggests that very little interaction of ionospheric plasma and cometary water vapor occurs. They believe that the wake of the comet would mix ionospheric plasmas and cause large localized variations in electron densities in the vicinity of the wake. They first located a small comet on the dayglow imagery then looked for this kind of perturbation. Though they checked over 26,900 sightings, only 1.2% displayed a reliable signature.

In another article (Frank et al. 1987a) of particular interest, Frank contended that an atomic hydrogen torus exists around the sun caused by the large population of small comets. This paper, which was actually a response to findings by Donahue et al. (1987), offered the strongest piece of supporting evidence for the small comet theory. To

summarize, it stated that the Voyager 2 spacecraft had detected unexpectedly high levels of Lyman-alpha radiation in the inner solar system. This correlated almost perfectly with Frank's predictions. Lyman-alpha radiation is emitted from atomic hydrogen. According to Frank, the photodissociation of water molecules from the FSC bodies after entering the earth's atmosphere and later escaping to space was the source of the interplanetary atomic hydrogen. Donahue believed the difference between what was predicted by Frank and what was measured by Voyager 2 was enough to leave considerable doubt that the small comet theory was correct. He did, however, claim the atomic hydrogen torus theory was valid but its source could be ordinary comets and meteors.

The validity of the Frank small comet theory is still largely unresolved. The search for hard evidence continues, but to date none has been obtained that could settle the issue.

Chapter 3

WATER VAPOR IN THE MESOSPHERE

Although water vapor is just a trace constituent above the tropopause it plays as important a role in the middle atmosphere as it does in the lower atmosphere albeit in a different manner. In this chapter, a review of our understanding of water vapor in the mesosphere will be given. Next, the impact of the small comet theory on the mesosphere will be discussed. Following this, the methods of observing mesospheric water vapor will be presented. Finally, the Penn State microwave radiometer will be discussed.

3.1 Current knowledge of mesospheric water vapor

Several research groups have made observations of the vertical, meridional, and seasonal distribution of water vapor throughout the mesosphere. Figure 3.1 (Olivero and Bevilacqua 1989) is a compilation of some of these data sets for the month of December. In Figure 3.1, five data sets were combined to produce a mean meridional-vertical cross section of water vapor throughout the middle atmosphere. These include the LIMS data set collected by the Nimbus-7 satellite (Remsberg et al. 1984) the GRILLE IR solar occultation data (Girard et al. 1988), the JPL and Penn State ground-based microwave radiometer data (Bevilacqua et

Observations - December

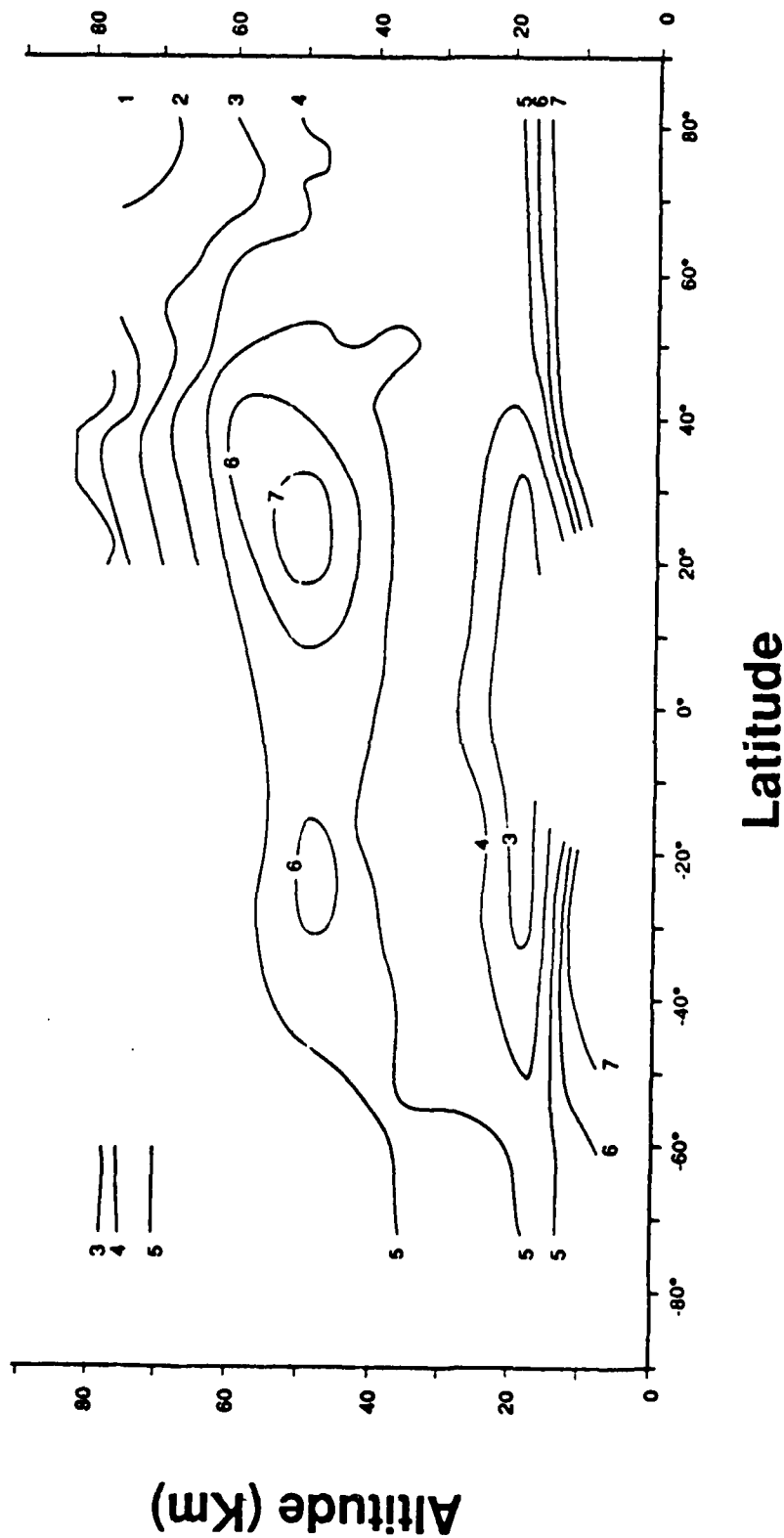


Figure 3.1: Vertical and meridional distribution of water vapor (mean values for December). Isopleth values are ppmv of water vapor. (Olivero and Bevilacqua, 1989)

al. 1989a), and airborne microwave radiometer data (Peter et al. 1988). This figure shows that the vertical profile of water vapor has maxima both in the troposphere, that being the main source region for water vapor, and near the stratopause due to methane oxidation. It also shows that minima exist in the lower stratosphere, due to dehydration caused by the atmospheric cold trap (to be discussed later), and in the upper mesosphere, caused by photolysis. The mixing ratios vary from between 2 and 3 ppmV at the minima to between 5 and 7 ppmV at the lower mesospheric maximum. The water vapor mixing ratios in the northern hemisphere also decrease with increasing latitude between 45°N and 75°N. Similar latitudinal data for the southern hemisphere has not yet been obtained.

Figure 3.2 (Bevilacqua et al. 1989b) depicts seasonal variations in mesospheric water vapor. In that study, Bevilacqua et al. showed that the Penn State ground-based radiometer data compared favorably with the JPL, ATMOS and GRILLE data sets as well as with the results of the study of seasonal variations of mesospheric water vapor by Thacker et al. (1981). These studies showed water vapor at all levels throughout the mesosphere following an annual cycle with low values in the winter and high values in the summer. In all years studied, water vapor increased from winter to summer about 1 ppmV at 65 km and 2.5 ppmV at 80 km. With these pieces of observational evidence, a picture of the processes

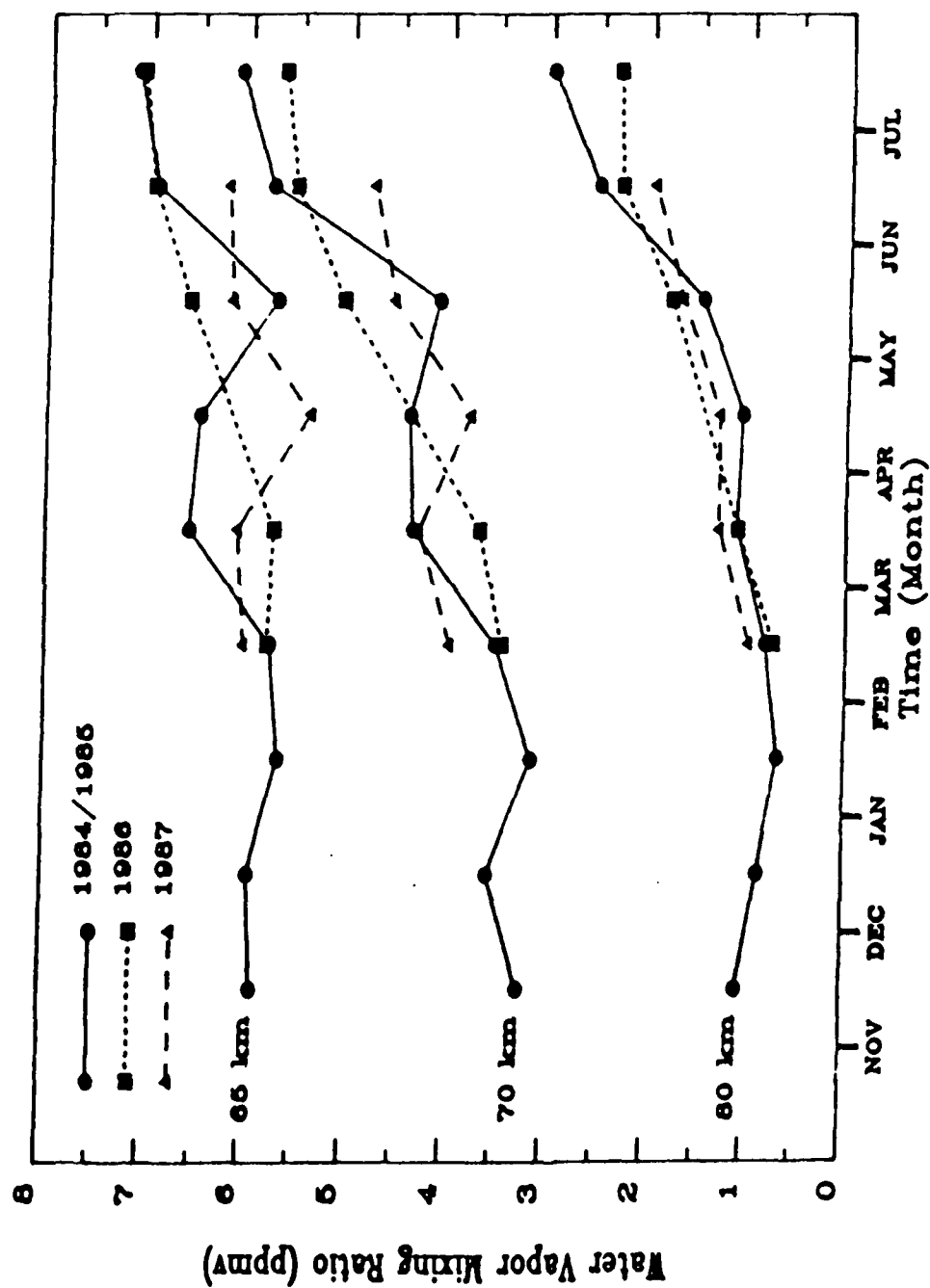


Figure 3.2: Season variations in mesospheric water vapor.
(Bevilacqua et al., 1989b)

affecting water vapor can be drawn.

It has long been thought that a primary source of water vapor for the middle atmosphere is the earth's surface (Dobson et al. 1946). Water vapor is advected upward through the tropopause over the tropics as a consequence of the Brewer circulation (Brewer 1949). Due to the extreme height and low temperatures at the tropical tropopause most of the water vapor is condensed out, greatly dehydrating the air moving into the stratosphere. In the stratosphere, various dynamic mechanisms carry water vapor into the mesosphere. In the mesosphere, a seasonal variation in vertical advection occurs. Water vapor is advected upwards in the summer and downwards in winter especially at middle to high latitudes (Murgatroyd 1969). This can account for both the increases in water vapor concentrations in summer and decreases in winter. Diffusive processes appear to be of secondary importance in the distribution of water vapor in the mesosphere (Bevilacqua et al. 1989a). Meridional transport is associated with horizontal differential heating caused by stronger absorption in the summer hemisphere thus causing westward flow in the summer hemisphere and eastward in the winter (Brasseur and Solomon 1984). Gravity waves and atmospheric tides also affect circulation in the mesosphere.

Photochemical sources and sinks are another important factor in interpreting water vapor observations of the

mesosphere. Water and its photolysis products (H , OH , O , H_2) are known to have important photochemical reactions with $\text{O}(^1\text{D})$, O_3 , CH_4 , NO_x , ClO_x , and a host of other gases in the mesosphere. These reactions can significantly change the water vapor concentrations in the mesosphere. The oxidation of methane is, perhaps, the most significant source of water vapor for the middle atmosphere. For a complete description of photochemical processes affecting mesospheric water vapor see Le Texier et al. (1988).

Water vapor is also important in the ion chemistry of the mesosphere. As mentioned earlier, increases of water vapor lead to increases of cluster ions, ionic species brought together by the strong electrostatic dipole of the water molecule. Cluster ions have a higher recombination rate than ordinary ions and thus deplete free electrons to a much greater extent. This therefore weakens the D-region of the ionosphere and alters radiowave propagation through the mesosphere (Tsou 1986).

Yet another consideration is water vapor's role as a greenhouse gas. Because water vapor is a strong absorber/emitter of longwave, radiation water plays an important role in the radiative balance, in establishing the temperature gradient, and therefore in helping determine the dynamics of the mesosphere.

The amount of water vapor present in the middle atmosphere also has a great impact on the presence of

noctilucient (polar mesospheric) clouds. These high altitude clouds have been linked to methane photochemistry (Thomas et al. 1989). Since the global atmospheric inventory of methane may be on the rise, the planetary albedo may increase as noctilucient clouds become more prevalent. Furthermore, noctilucient clouds provide surfaces on which heterogeneous chemistry may take place.

3.2 The impact of small comets on mesospheric models

Current models of mesospheric water vapor do not sufficiently explain recent observations (Bevilacqua et al. 1989b). The Penn State water vapor measurements show a particularly dry mesosphere over long periods (days to years). The loss mechanisms employed in the models (vertical transport and photochemical processes) would appear to be too small to dehydrate the mesosphere to the observed long-term average conditions.

Furthermore, if the small comet theory were true, the models would be neglecting a new, potentially large, source of water vapor for the mesosphere. This proposed extraterrestrial source would produce a downward flux of 3×10^{11} H_2O molecules $\text{cm}^{-2} \text{sec}^{-1}$ which equates to a 5.0×10^{37} H_2O molecules/year potentially entering the mesosphere (Reid and Solomon 1986). This annual source is three times the estimated total number of water vapor molecules in the

mesosphere. The loss mechanisms used in the present mesospheric water vapor models would not be able to balance such a large source.

Whenever a major scientific hypothesis is proposed which strongly challenges a large body of theory and observations, it is incumbent on individual scientists to examine their own measurements and theories in an attempt to either support or refute the new hypothesis. That is the basis of the present study.

3.3 Methods of observing mesospheric water vapor

Observations of water vapor concentrations in the middle atmosphere have been made by both in situ and remote sensing systems. Most of the in situ experiments have employed balloon or rocket-borne measurement devices. Due to the very low atmospheric density of the mesosphere, balloon based probes are incapable of penetrating the stratopause. Scholz et al. (1970) were first to obtain mesospheric water vapor measurements using a rocket-borne cryocondenser. Other successful rocket-borne in situ systems include coulometric humidity sensors (Fedynski and Yushov 1980), and mass spectrometers (Arnold and Krankowsky 1977). Generally, the water vapor amounts given by early in situ methods were much higher than expected, probably as a result of the outgassing of water vapor from the instruments

themselves. Due to this difficulty, the relative high cost of rocket based experiments, and the short period of observations they provide, in situ methods have received very little use.

Remote sensing of mesospheric water vapor has been conducted using absorption and emission of both infrared and microwave radiation. The infrared measurements have been taken from rocket-borne spectrometers and photometers as well as satellite based radiometers. Microwave measurements were first obtained by Radford et al. (1977) using a ground-based radio telescope. Airborne microwave radiometers have also been successfully used to retrieve mesospheric water vapor profiles (Waters et al. 1980; Kunzi et al. 1983; and Peters et al. 1988). The advantage of ground-based microwave radiometers becomes clear when considering the Penn State data base. The relatively low cost system has been providing mesospheric water vapor profiles since 1984, making it the largest data set of its kind. For a complete review of mesospheric water vapor observations refer to Bevilacqua (1982) or Tsou (1986).

3.4 The Penn State microwave radiometer

In evaluating the usefulness of the Penn State radiometer data base in the search for evidence concerning

the small comet theory, several points should be considered. It is the only continuous (or semi-continuous) record of mesospheric water vapor available in the world. It monitors a region of the atmosphere (the mesosphere and lower thermosphere) which should be affected by the influx of extraterrestrial water (Frank et al. 1986b). Also, the observations concentrate on a small, specific solid angle of the sky. This fixed geometry permits the probability of detection to be estimated easily (Adams 1988). The data base also extends over a very long period of time (approximately 500 days of useable data up to the end of 1988); thus if the phenomenon exists, the probability that these observations would lead to detection is very good. Because of these unique attributes, the Penn State radiometer water vapor data base is well suited for making inferences concerning the existence of this extraterrestrial water vapor source.

There are basically three main components to the Penn State spectral radiometer: the antenna, the receiver, and the "back end" consisting of the spectrometer, signal conditioning circuitry, output/archival system and the microprocessor (control computer). The antenna used is a 24-inch pyramidal horn mounted vertically under a movable, planar aluminum reflector. The antenna beam ($\sim 5^\circ$ halfwidth) can be pointed toward any azimuth and over a large range of elevation angles. The beam is usually

directed toward the northeast with an elevation angle of 10° to 30°.

Let us consider the interaction between microwave radiation and the radiometer. In a receiver operating at some physical temperature, T , above absolute zero, fluctuations of the output are caused by the random thermal motions of electrons within the electronic components. These fluctuations generate a noise power given by the expression (Nyquist 1928):

$$P = kTB \quad (3.1)$$

where k is the Boltzman constant

T is the physical temperature of the electrical components, and

B is the bandwidth over which the power is measured. When the radiative power of the atmosphere incident upon an antenna is being measured by electronic equipment, a "brightness temperature" of the atmosphere can be obtained using equation 3.1. Because the antenna used is nearly 100% efficient, T_a (antenna temperature) characterizes the atmospheric brightness temperature, T_{sig} , (signal temperature). Similarly, the receiver has a characteristic noise power caused by the individual electronic components which is expressed as the receiver temperature, T_{rec} . The sum of the receiver and signal temperature determine the system temperature T_{sys} which is that power output from the

entire system in response to radiation incident on the antenna.

In order to extract information from the system the signal-to-noise ratio must be sufficiently high. In this system, the "signal" is proportional to T_{sig} and the noise is proportional to T_{rec} , therefore T_{sig}/T_{sys} is approximately equal to the signal/(signal+noise). Since the incident radiation has a power of around 10^{-20} watts (Tsou 1986) it is very important to have a low noise receiver. This is achieved (in the Penn State receiver) by use of an extremely low noise, cryogenically cooled MASER which amplifies the signal immediately after it leaves the antenna. Steinberg and Lequeux (1963) showed that receiver noise is largely determined by the noise output of the first electronic component of a receiver. Thus, the MASER performs the crucial function of improving the systems signal to noise ratio.

The signal output from the MASER still requires further amplification in order to be useful. Such additional gain is more easily accomplished at frequencies much lower than the 22.235 GHz signal frequency. Therefore, a process called superheterodyning (or mixing) is used. Referring to Figure 3.3 the output signal from the MASER is mixed with a signal at 22.175 GHz produced by a local oscillator in a component called a mixer. Here, the sum and difference (or beat frequency) of the two signals at 44.400 GHz and at 60

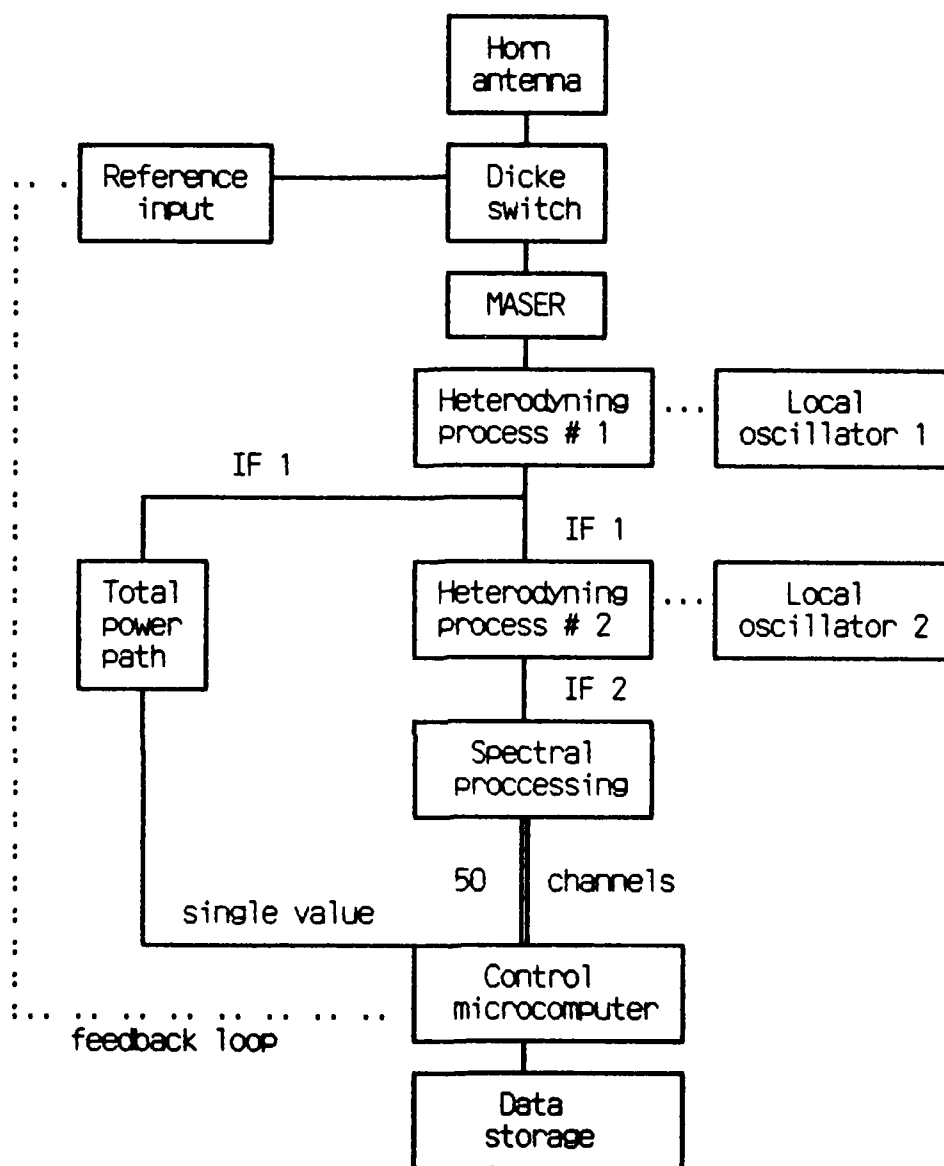


Figure 3.3: Penn State microwave radiometer block diagram

Mhz are produced. A band/pass filter then eliminates the summed frequency leaving the difference frequency, now referred to as intermediate frequency 1 (IF_1). At this point IF_1 is split into two paths. One path leads to the total power amplifier which steps up the signal amplitude so that it may be detected and recorded. The detection is performed by a square law detector in which output voltage is proportional to input power. Again, as a consequence of equation 3.1, the output voltage from the square law detector is proportional to the signal temperature. The task of recording will be discussed later.

The second path from the splitter leads IF_1 through a second heterodyning process and amplification. The resulting intermediate frequency 2 (IF_2) enters a parallel filter bank and is divided into 50 channels of 50 KHz each. The theoretical peak of the spectral line is centrally located within these 50 channels. Each channel output passes through a square law detector like that in the total power path. The output voltages are then collected in 50 separate integrators for a period of 1/4 second. These analog signals are dumped through an analog/digital converter to the microcomputer where they are compiled into 20 minutes integrations. The ensemble of 50 digital outputs are recorded along with the output from the total power path by a microcomputer along with the time of the data dump on floppy disks.

In addition to the atmospheric radiative source collected by the antenna, a reference source of radiation is measured by the system. Due to the instability of the electronic devices, the gain of the system may change with time. In order to correct for these gain fluctuations, the input to the system is constantly switched between the antenna and a reference input (a thermal load). This reference input is provided by a 4°K cold station in the cryogenic system which is connected through a variable attenuator to the switching device at the input end of the system. This allows the cold load to closely simulate the brightness temperature of the sky. The signal that is actually analysed by the system is then a difference between the sky and the reference temperatures. This difference appears as a linear offset in the raw data which varies from one 20 minute spectrum to the next.

This approximation to the sky temperature is accomplished by a feedback loop in the computer software. It is important that the reference temperature be close to the sky temperature since switching between two dissimilar temperatures can cause nonideal responses in the electronic sensing components. The switching rate must be shorter than any typical gain variations and was chosen to be 1 cycle per second. This type of amplitude switching is called Dicke switching after the person who first suggested its use (Dicke 1946).

The system is periodically calibrated by measuring a noise source of known value. The calibration temperature, (T_{cal}), is used to scale the noise power value in equation 3.1 to obtain the actual atmospheric brightness temperature. This procedure is used to counter fluctuations in the system's gain. For simplicity, brightness temperatures computed for this study use a T_{cal} of 1°K. Actual system calibration temperature range between 2°K and 4°K. The relative brightness temperatures reported, therefore, are 1/2 to 1/4 the actual value.

Chapter 4

THEORETICAL CONSIDERATIONS

The mesospheric and thermospheric water vapor data used in this study were collected by the remote sensing of the 22.2 GHz water vapor resonance line by a ground based microwave radiometer system located at the University Park Campus (41°N, 78°N) of Penn State. In order to interpret this data, it is first necessary to understand the basic theoretical considerations involved in obtaining and extracting useful information from the raw data. This chapter first discusses the equation of radiative transfer as it relates to the thermal emission which is measured by the radiometer. Then the concepts of spectral line broadening are covered. Lastly, the process by which water vapor concentration profiles are extracted from these spectra is presented.

4.1 Radiative transfer equation

A radiometer is a device which can measure the intensity of radiation incident upon it, but without a clear understanding of how that radiation was transmitted to that device, the raw data is meaningless. The equation of radiative transfer describes how the intensity of radiation generated by an extended source changes as it travels toward the receiver.

The optical depth, $\tau(\nu, s, 0)$, is a function of frequency, ν , and path length, where $s=0$ is the position of the radiometer and s is an arbitrary point above the radiometer. The optical depth may be written as:

$$\tau(\nu, s, 0) = \int_0^s K(\nu, s) ds \quad (4.1)$$

where, $K(\nu, s)$ is the extinction coefficient and s is measured along the atmospheric path of interest. Extinction can be thought of as the attenuation of a beam of radiation by scattering and absorption. For microwave radiation in the atmosphere, scattering is small compared to absorption and can be neglected. Thus, $K(\nu, s')$ is similar to the absorption coefficient $K_a(\nu, s')$ at frequency ν and position s' .

Because the atmosphere is in local thermodynamic equilibrium (LTE) at the altitudes of interest and the Rayleigh-Jeans approximation of the Planck function is valid (Waters 1976), the equation of radiative transfer can be written as:

$$T_g(\nu) = T_\infty(\nu) \exp(-\tau(\nu, \infty, 0)) + \int_0^\infty T(s) \exp(-\tau(\nu, s, 0)) K_d(\nu, s) ds \quad (4.2)$$

where $T_g(\nu)$ is the brightness (equivalent blackbody) temperature, at frequency ν , of the radiation measured at the ground.

$T_\infty(\nu)$ is the brightness temperature, at frequency ν , of the background (or a practical source such as the sun or moon).

$T(s)$ is the local kinetic temperature of the atmosphere at a distance s from the receiver.

$K_a(v, s)$ in this form is the atmospheric emission coefficient, at frequency v , and location s (as a consequence of Kirchoff's Law which states: absorptivity equals emissivity).

In this case, $T_\bullet(v)$ is the cosmic background temperature (2.7°K) which is small compared to the source function (the second term on the right side of equation 4.2) and is usually considered insignificant. For absorption measurements an antenna would be aimed at an extraterrestrial source (e.g. the sun) and the first term of equation (4.2) would be the more important of the two.

The absorption coefficient, $K_a(v, s)$, can be expressed as the water vapor number density, n , times the absorption cross-section, $\sigma(v, s)$, where σ varies with height due to pressure broadening. Thus, equation 4.2 becomes:

$$T_g(v) = \int_0^\infty T(s) \exp(-\tau(v, s, 0)) \sigma(v, s) n(s) ds \quad (4.3)$$

This equation is used in this study to describe the spectral line radiation reaching the antenna. Because the antenna of the Penn State radiometer has an efficiency of nearly 100%, $T_g(v)$ is essentially equal to the antenna temperature.

4.2 Spectral line broadening

If the atoms and molecules of a certain species were motionless and isolated from each other the resonant energy lines would be very narrow. Only natural line broadening would prevent the energy from being absorbed and emitted at a single, specific frequency (Liou 1980, p 16). Because motion and interaction do occur, these lines become broader i.e. radiation is emitted and absorbed over a range of frequencies about the center (resonant) frequency. The two main broadening processes are called Doppler broadening and pressure broadening.

In Doppler broadening, frequency shifts (Doppler shifts) occur due to the brownian motion of atoms and molecules which are at temperatures above absolute zero (0°K). Because the molecules are randomly moving, most will have velocity components toward or away from the remote sensor. These motions cause Doppler shifts toward both higher and lower frequencies, which are a function of the square root of the ambient temperature at the radiation source.

When a molecule undergoes a collision with another body, the entire energy structure is perturbed momentarily, and the energy required to absorb or emit a photon can change. Therefore, the frequency of the emitted photon is altered. The rate of collisions is proportional to the

pressure (and a weak function of temperature) and thus the process is called pressure broadening.

When pressure is relatively high, pressure broadening is the dominant process. At levels above about 95 Km, Doppler broadening becomes dominant for the 22.2 GHz line. In the transition altitudes, from 75 - 95 km, both are important. The Voigt line shape function, a combination of the Doppler and pressure broadening effects, provides a solution for the broadening of resonant lines at these altitudes. For a complete discussion of spectral line broadening see Longbothum (1976).

4.3 Inversion of spectral data

Because of this primary dependence on pressure (with a much less important temperature dependence) vertical profiles of the constituent's concentration are obtainable from the spectral line data. This process of information extraction is called (data) inversion. Data from this and many other remote sensing problems can be inverted by solving an equation of the form:

$$g(v_1) = \int N(v_1, x) f(x) dx \quad (4.4)$$

where: $g(v_i)$ is the measured radiation at frequency v_i
 $f(x)$ is the desired information at location x
 $W(v_i, x)$ is the Kernel or weighting function of v_i
 at location x , which relates $g(v_i)$ to $f(x)$.

Equation 4.4 can be approximated, using numerical methods by an equation of the form:

$$g(v_i) = \sum_{j=1}^n W(v_i, x_j) f(x_j) \Delta x_j \quad (4.5)$$

The evaluation of equation 4.5 would yield a family of equations which could be expressed as:

$$g = W f \quad (4.6)$$

where g and f are vectors of length n and m and W is an $(n \times m)$ matrix.

The obvious first order solution for f is:

$$W^{-1} g = f \quad (4.7)$$

However, this seldom works for real radiative transfer problems because the matrix W is usually singular or nearly so. Many special solutions have been developed for this problem but are beyond the scope of this study. Refer to Twomey (1975) for details.

Physically, two factors control the shape of the weighting functions. Photons of a given frequency emitted at the highest levels are joined by those emitted at lower levels as they travel downward towards the radiometer. An increasing amount of absorption also occurs due to the ever increasing concentration of absorbers along the downwards

path. A peak intensity is reached below which photons absorption dominates and above which photon emission dominates. This describes a very smooth bell-shaped function. Because the frequency separation between the weighting functions is small, they tend to overlap rendering the inversion matrix nearly singular. Without special inversion techniques even small amounts of noise in the data "g" would cause large errors in the retrieved solution vector "f." If we compare the inversion equation (equation 4.4) to equation 4.3 we find that $T_g(v)$ is represented by "g" and $n(s)$ is $f(x)$, therefore the weighting function can be written as:

$$W(v, s) = T(s) \exp(-\tau(v, s, 0)) \sigma(v, s) \quad (4.8)$$

A problem arises here because in order to find $W(v, s)$, τ must first be known. and τ depends on the vertical water vapor concentration which we seek. However, the largest contribution to the optical depth, τ , is made by the troposphere. Due to the effect of pressure broadening on the resonant frequency the tropospheric signal is extremely broad and flat while the mesospheric signal is only weakly pressure broadened. The mesospheric signal appears as a very narrow, low amplitude peak centered on the resonant frequency. When examining the mesospheric signal in detail the tropospheric signal appears so wide and flat that it can be subtracted off leaving the mesospheric signal virtually undistorted. With this understanding equation 4.8 can be

approximated as:

$$N(\nu, s) = T(s) \exp(-\tau(\text{trop})) \sigma(\nu, s) \quad (4.9)$$

where the optical depth of the troposphere, $\tau(\text{trop})$ is defined as:

$$T(\text{trop}) = \int_0^{\text{tropopause}} K_d(\nu, s) ds \quad (4.10)$$

This parameter, $\tau(\text{trop})$, must be estimated either from the system itself or from independent atmospheric data (see Tsou 1986 for details).

The details of the inversion process are beyond the scope of this study but are thoroughly described by Bevilacqua (1982) and Tsou (1986).

Chapter 5

EXPERIMENTAL PROCEDURES

Data from the Penn State microwave radiometer have been analyzed by many researchers over the past few years. Many of the experimental procedures employed in this study have been previously developed, tested, and proven effective. Although most of the data analysis procedures have been used before, some newly developed methods were also employed in this study.

The purpose of this chapter is to familiarize the reader with both the newly and previously developed data analysis procedures. This chapter will first outline how the data is prepared for analysis. Next, the basic data analysis procedure will be discussed. Following this, the procedures for detecting unusable data will be reviewed. Finally the procedure for identifying 20-minute water vapor concentration increases possibly caused by small comets will be presented.

5.1 Data preparation and handling

The radiometer output undergoes a fair amount of preparation and handling prior to analysis. In its normal operation, the back end microprocessor of the radiometer system dumps raw data to 5 1/4 inch disks every 20 minutes.

When filled, these disks will contain about one week's worth of data in track and sector format. This information is then manually transformed into APPLE system files, then converted into IBM PC format. These files, containing one day's data, are then sent via a high speed data link to the Penn State Center for Academic Computing facility's IBM mainframe computer. The entire available data base (approximately 500 days from the period Nov. 84 to Sep. 88) is stored on magnetic tape archives and retrieved in small sections for processing. In this way original data can always be restored from the archives or from the original 5 1/4 inch floppy disks.

Newly developed software includes the Apple program "BUILD5" (used to convert track and sector data to data files) and the "Core Analysis Program (CAP FORTRAN)" (used to perform all data analysis and the search for small comets). Commercial software is also used for graphics and statistical processing.

5.2 Analysis procedures

Theoretically, a water vapor spectrum should appear as a smooth curve increasing from the greatest offset frequencies to a maximum value at the center, resonant frequency (22.235 GHz). Actual 20-minute spectra, however, are noise dominated because the signal being sensed is very

weak (Tsou 1986). In addition to this, the spectra usually display both linear and nonlinear baseline effects making them asymmetric.

The signal to noise ratio in a 20-minute spectrum can be improved by a method called folding. Because the molecular line is inherently symmetric about the line center information from equally offset frequencies can be averaged to reduce the noise in the resulting "folded" channel. Averaging the output from channels 24 and 26, 23 and 27, etc. (folding), not only improves the signal-to-noise ratio of the folded channels, but also removes linear and other odd order baseline effects. For more on the removal of baseline effects see Bevilacqua (1982).

Another procedure for improving data quality is to integrate over longer periods of time. Noise, being randomly distributed about the signal, decreases as the square root of the sampling time (integration period) increases. In the past, the 12-hour integration has proven to yield a sufficient signal to noise ratio for reliable inversion (Tsou 1986). In this study, the 12-hour integration is used as a standard of comparison for the 20-minute spectrum which contributes to it.

It is also necessary to determine the variability of data within each channel in the 12-hour integration. Channel standard deviations for both the folded and unfolded 12-hour integration give an indication of the amount of

noise compared to signal. With this initial information concerning the 20-minute and 12-hour spectra, judgments of data quality can be made.

5.3 Unusable data identification

Although all the 20-minute spectra contain a certain amount of noise, some have an overwhelming amount. There are generally two causes for extremely poor signal-to-noise ratio spectra. The first of these are local interference caused by radio and other sources. The second being a reduction of the mesospheric water vapor signal caused by strong attenuation in the troposphere. Rain is the leading cause of strong tropospheric attenuation.

These two causes of poor quality data have very different effects on the spectra. Isolated "spikes" in the spectra can be caused by stuck channel values coming from poor connector contacts in the printed circuit cards of the filter bank. High tropospheric attenuation affects every channel in the spectrum. As a result, the mesospheric signal is completely lost, leaving the affected spectra unusable.

If a number of 20-minute spectra display these effects, the 12-hour integration spectrum and variances to which they contribute may also become unusable. In the past, identifying unusable data was subjectively done by hand.

The process required a great deal of effort and attention by a person who was very familiar with the data. Now, a series of tests based on the 12-hour integration, variance and 20-minute spectra are used by the Core Analysis Program to identify unusable data.

As a result of these tests, isolated channel spikes may be flattened to conform with adjacent channels, 20-minute spectra may be marked as unusable, or entire 12-hour series of 20-minute spectra may be marked as unusable. Once a spectrum is marked unusable, it will be excluded from subsequent processing, thus constraining the impact of its nonphysical information. All actions to correct or mark unusable data are documented for later review and possible revision. It is important to note that these procedures do not affect the archived data base, only the copy of the archived data being examined.

After unusable data is marked, the 12-hour integration and variances are recomputed excluding the unusable data. The data used to search for small comet events are these qualified data.

5.4 Search procedures

The search for anomalously large water vapor concentrations, possibly caused by the introduction of extraterrestrial water vapor into the radiometer beam

(hereafter referred to as an event), is a two step data analysis procedure. The first step is to make a preliminary identification of an event. The second step is to investigate these data sets with more thorough statistical tests.

The Core Analysis program performs a standard Z test (see chapter 6) on all usable data. If the two center channels of a folded 20-minute spectrum display values more than 1.5 standard deviations above the 12-hour integration mean for these channels, that spectrum is marked for further investigation.

The second interrogation of these possible event spectra uses a Student T test (see chapter 6). Here, the center three channels of the suspect spectra are tested at the 0.05 alpha level. Those spectra passing this criterion are considered (event) detections. They are examined individually and are reported in this study.

Unlike the initial Z test that uses fixed 12-hour data, the second test uses a more flexible data block. This block is compiled such that the 36 temporally closest 20-minute spectra to the suspect spectrum are selected. If unusable data is encountered during this compilation process it is skipped and scanning continues until 36 usable spectra are selected. The subroutine will examine a maximum of 74 spectra in an attempt to obtain 36 usable spectra. If fewer than 36 usable spectra are obtained, processing continues

with this reduced set. This series of 36 (or less) spectra is used for the event detection procedure.

Once spectra are identified as events, spectra adjacent to these are examined by reviewing the Z test results to determine whether the event is an isolated occurrence. A small comet should affect at most two consecutive 20-minute spectra and usually only one (Adams 1988).

Chapter 6

STATISTICAL CONSIDERATIONS

It is obvious from the previous chapter that the results of this study are greatly dependent upon many statistical procedures. The purpose of this chapter is to clearly establish the statistical basis of the study. This chapter first discusses the folding and integration procedures from a statistical point of view. Next the Z test and test for normality of the data set are presented. Finally, the newly developed procedure for selecting 20-minute observations as small comets events is explained.

6.1 Folding and integration

As mentioned in chapter 5, two methods for improving the signal-to-noise ratio of the data are first, integrating many 20-minute spectra into one spectrum of longer period and second, folding these spectra about their central frequencies. In both cases, more data points are being used to improve the estimation of the value being sought. In statistics, this concept is expressed as the Central Limit Theorem.

In short, the Central Limit Theorem states that as the number of pieces of information contributing to a point estimate (be it an average value or variance value) increases, the point estimate will asymptotically approach

the true value being estimated. The Central Limit Theorem also states that as the sample size increases the distribution of these values will more closely resemble a normal distribution (Devore 1987, pp. 212-216). It is for this reason the noise is decreased by the folding and integration processes.

Some care must be taken, however, when variances are calculated from folded data. Because of the baseline effects, which tends to make the values of channel equally offset from the center frequency unequal, the estimate of the variance has to be a "pooled" sample variance (Devore 1987, p. 335).

$$s_p^2 = \frac{(n_a-1)S_a^2 + (n_b-1)S_b^2}{n_a + n_b - 2} \quad (6.1)$$

Here, n_a and n_b are the sample sizes for the channels being folded and S_a^2 and S_b^2 are the respective variances. Since for our case n_a always equal n_b , equation 6.1 reduces to:

$$s_p^2 = \frac{(S_a^2 + S_b^2)}{2} \quad (6.2)$$

It would appear that as a consequence of the Central Limit Theorem the variances calculated from folded data will always be a better estimator of the data variability than variances calculated from unfolded data. However, a problem arises in the center channel (channel 25) which during the folding process is unpaired. For every other channel a

counterpart channel, equidistant from the center channel, exists. When these paired channels are linearly combined a smaller variance is obtained as a result of the Central Limit Theorem.

Because channel 25 data is unpaired by other data as with the other channels, the variance of its folded integrated value can be greater than other channels with identical distributions. Depending on the correlation structure, the estimated value may be between 1 and 1.4142 times greater than the actual value (Devore 1987, pp. 484-487). This discrepancy is completely alleviated, however, when standardized values are used as will be described later in this chapter.

6.2 The Z and normality tests

The Central Limit Theorem provides a powerful tool for understanding how data quality, as measured by the signal to noise ratio, improves as the number of data points increases. It also implies that we can expect the data set to follow a normal distribution. Since many of the statistical procedures depend on the data being approximated by a normal distribution, it is worthwhile to test this hypothesis.

As mentioned in Chapter 5, a Z test is conducted on all usable 20-minute spectra. The test is performed by finding:

$$Z = (OBS - INT) / STD DEV$$

6.3

where Z is the test statistic

OBS is the value of the channel output on a 20-minute observation

INT is the value of the channel output on a 12-hour integration

and STD DEV is the standard deviation for the channel over the 12-hour period of integration.

The Z statistic is computed for channel 25 and 26 data and compared to 1.5 standard deviations. If the Z statistic for both channels exceed 1.5 standard deviations, the 20-minute spectrum is submitted for further processing. In a noise dominated spectrum, values of consecutive channels are unrelated (independent). Thus, the probability of obtaining a spectrum that meets the forementioned criterion is:

$$(P_{21.5})^2 = (0.0668)^2 = 0.445\%$$

6.4

These Z statistics can also be used to determine if the data is normally distributed. Once the Z statistics were calculated a random sample was taken from several months of data. This sample, consisting of 1,000 20-minute observations, was then plotted against a corresponding normal distribution. Figure 6.1 displays the results of the normality test. A perfectly normal distribution will be a straight line with a slope of 1 and intercept of 0. The results indicate that the data set is well estimated by a

Normality Test

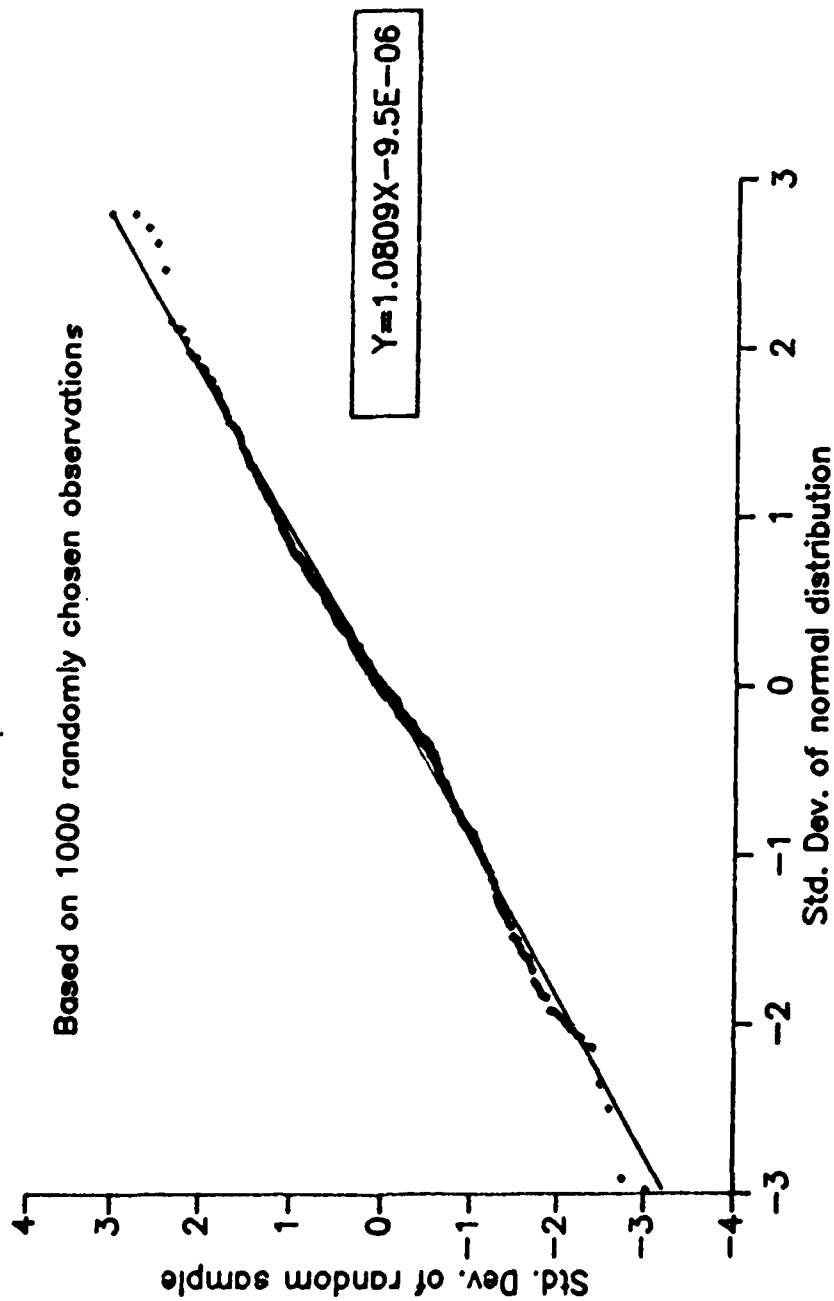


Figure 6.1: Results of the test for normal distribution including the linear regression equation

normal distribution.

The effect of a poorer fit to the normal distribution would not necessarily invalidate the test procedures, however. The probabilities would certainly be less reliable but underlying theory would not be compromised (Miller and Freund 1977, p. 108).

6.3 Event detection

Section 5.4 describes the procedure used to search for events. There are several important statistical considerations involved in this procedure.

As mentioned earlier, the 20-minute observations used to form a group of 36 spectra are selected such that the suspected event spectrum is temporally centered within, but excluded from, the group of 36 observations. This closely follows the concept of a confidence interval. In a confidence interval, limits are set on a group of data in order to bracket, with a certain probability, a zone where the next selected data point should fall (Miller & Freund 1977, p. 186). The point being examined is excluded from the interval so that it can not influence the interval. The purpose for trying to center the point is a consequence of the assumption that the change of water vapor concentration with time should be a smooth function and the best point estimator is the centered point in the interval (Devore

1987, pp. 225-227).

Another important statistical concept being employed is the hypothesis test. A hypothesis test uses a test statistic to determine the validity of a pre-stated hypothesis at a certain alpha level (confidence level).

The hypothesis we are testing is that data in consecutive channels of the suspect spectrum are dependent upon each other. This is only true when signal dominates that portion of the spectrum being tested. In other words, the test statistics relates to the probability that the suspicious spectrum was generated purely by chance (noise).

For our application, the Student T test statistic is used. It is based on a Gaussian probability distribution function similar to the normal distribution. The Student T distribution is usually used when the number of data pieces is relatively small (36 for our case).

The test statistic is calculated as follows:

Let X_{25} , X_{26} , and X_{27} be the observed values on channels 25, 26 and 27 of the suspect spectrum.

Let \bar{X}_{25} , \bar{X}_{26} , and \bar{X}_{27} be the 12 hour integration for these channels.

and Let S_{25} , S_{26} , and S_{27} be the standard deviations for these channels.

Then

$$t_{25} = \frac{X_{25} - \bar{X}_{25}}{S_{25} (1+1/n)^{1/2}} , \quad t_{26} = \frac{X_{26} - \bar{X}_{26}}{S_{26} (1+1/n)^{1/2}} , \quad t_{27} = \frac{X_{27} - \bar{X}_{27}}{S_{27} (1+1/n)^{1/2}} , \quad (6.5)$$

where n = the number of observations comprising the integration period (usually 36).

t_{25} , t_{26} , and t_{27} are test statistics from independent T distribution with $n - 1$, $2(n - 1)$, and $2(n - 1)$ degrees of freedom respectively.

Probabilities for these test statistics are found using an IMSL subroutine for Student T distributions and are multiplied together to yield a P-value. The meaning of this P-value is that it is the probability the spectral characteristics tested were produced by random noise. This P-value is then compared to the alpha level of the hypothesis test. The alpha level is the level of confidence we wish to place in the hypothesis test. It is the probability of claiming that a spectrum was not produced by random noise when, in fact, it was. We have chosen an alpha level of 1.25×10^{-4} which corresponds to 5% chance for error in each of the three center channels. If the P-value is less than the alpha level, the null hypothesis (ie. the spectrum was generated by noise) is rejected and we claim to have found an event.

Chapter 7

RESULTS AND DISCUSSION

The period of record and a brief description of the data set are given in this chapter. Following this, the detected events of unusually high water vapor concentrations are presented. Next, case studies of several, selected events are presented. Then tests of system capabilities and the reliability of the data are discussed. Finally, a search for alternative explanations for the events is presented.

7.1 The data

The data used in this study were generated by the Penn State microwave radiometer during the period November 1984 through December 1988. Over 22,000 20-minute observations from over 500 days were used in the analysis.

Table 7.1 is a listing of the periods during which observations were being recorded. This is the data set used in this study. It is important to note that the data set is fragmented to a large degree. This is a consequence of the poor observing conditions due to bad weather, maintenance periods, and other planned and unplanned down periods.

In addition to the data gaps reflected in Table 7.1, smaller gaps ranging from 20-minutes to several days are

Table 7.1: Period of Record

Year	Month	Dates Inclusive
1984	NOV	13 - 19, 22 - 30
	DEC	1 - 12, 15 - 18, 20, 22 - 28, 30 - 31
1985	JAN	1 - 3, 10 - 19, 24 - 30
	FEB	1 - 11, 16 - 26, 28
	MAR	1 - 31
	APR	1 - 9, 11 - 19
	MAY	1 - 2, 6, 9 - 17
	JUN	1 - 15, 18 - 29
	JUL	1 - 23
1986	FEB	16, 23 - 28
	MAR	1 - 2, 12 - 25
	MAY	8 - 13, 19 - 29
	JUN	4 - 10, 12, 18 - 30
	JUL	2 - 3, 7 - 12
1987	FEB	7 - 15, 17 - 27
	MAR	2 - 10, 16 - 29
	APR	16 - 23, 26 - 30
	MAY	1, 3 - 6, 12 - 15, 20 - 31
	JUN	2 - 7, 9 - 11, 14 - 15, 23 - 30
	JUL	1, 3 - 8, 11 - 20
1988	APR	19 - 22, 24 - 28
	MAY	3 - 4, 10 - 15, 19 - 22, 26 - 29
	JUN	9 - 20, 22, 24 - 25, 28 - 30
	JUL	1 - 6, 13 - 15, 25 - 30
	AUG	1 - 18
	SEP	8 - 11
	OCT	6 - 16, 18, 20 - 31
	NOV	1 - 2, 9 - 10, 21 - 30
	DEC	1 - 3

present as a result of the analysis procedure which omits the poorer quality data.

7.2 The detected events

A 20-minute observation is identified as an event if it meets the criteria delineated in section 5.4 of this thesis. It is believed that the short-term peaks in brightness temperature are associated with temporary increases of water vapor being sensed by the radiometer.

Table 7.2 is a listing of the 111 events detected within the period of record. It lists the date and time of the event, and the P-value of the event which is a measure of likelihood by chance.

7.2.1 Low resolution time line

Figure 7.1 is a low resolution time line which depicts the period of record and the frequency of occurrence of the events. Its purpose is to illustrate the entire data set and when events occurred. It clearly shows the fragmented nature of the data set and the seemingly sporadic nature of the events with respect to time. It also shows that observations were usually not taken during the late summer and autumn months due to the anticipation of poor observing conditions. The underlined periods (23-28 FEB 1986, 1-2 MAR

Table 7.2: Summary of Detected Events

YY/MM/DD	Time	P-value	YY/MM/DD	Time	P-value	YY/MM/DD	Time	P-value
84/12/04	0500	2E-5	85/07/11	2220	3E-6	87/05/31	0940	2E-5
84/12/17	1500	4E-6	85/07/13	0540	4E-6	87/06/02	2240	3E-7
85/01/03	2300	1E-7	85/07/18	2020	9E-6	87/06/05	0800	1E-4
85/01/13	1140	3E-5	86/02/16	1720	2E-28	87/06/06	2220	1E-5
85/01/20	0500	9E-6	86/02/28	0020	4E-7	87/06/07	0920	3E-5
85/01/30	1500	6E-5	86/03/01	1700	4E-5	87/06/10	0700	7E-7
85/02/18	1500	2E-5	86/03/01	2040	2E-5	87/06/11	0540	3E-6
85/02/22	0700	5E-8	86/03/18	0320	1E-6	87/06/24	1600	5E-5
85/03/12	0100	2E-7	86/03/19	1220	1E-4	87/06/25	1200	2E-5
85/03/15	1340	2E-5	86/03/19	1500	4E-5	87/06/27	0520	7E-5
85/03/15	2220	5E-6	86/03/22	0720	6E-5	87/07/01	0120	1E-6
85/03/18	1800	1E-4	86/03/22	1020	4E-5	87/07/01	0420	2E-5
85/03/19	2240	1E-5	86/05/09	2340	8E-5	87/07/08	0940	2E-5
85/03/31	1700	1E-5	86/06/21	2200	9E-5	87/07/08	1240	5E-5
85/04/14	0620	4E-5	86/06/22	1220	1E-5	87/07/08	2000	1E-5
85/04/14	1600	1E-6	86/07/03	1520	2E-5	87/07/18	1220	4E-5
85/04/14	1720	3E-5	87/02/07	1840	3E-5	87/07/19	0940	1E-5
85/04/18	1920	4E-5	87/02/11	1200	5E-5	88/05/15	2340	2E-6
85/04/18	2140	5E-5	87/02/18	0500	1E-4	88/05/28	1800	4E-5
85/05/02	1740	4E-6	87/02/26	0740	7E-6	88/06/10	0500	8E-5
85/05/10	1840	1E-5	87/03/08	0940	1E-4	88/06/10	0540	2E-5
85/05/10	2320	4E-7	87/03/19	2020	6E-5	88/06/10	2220	7E-5
85/05/11	0920	2E-6	87/03/21	0620	4E-5	88/08/10	1200	3E-5
85/05/12	2220	4E-5	87/03/21	0720	4E-7	88/08/16	2100	8E-5
85/05/16	0620	9E-6	87/03/23	2240	2E-5	88/08/18	1400	2E-5
85/06/03	0320	1E-5	87/03/27	1300	7E-6	88/08/18	1920	7E-5
85/06/06	2020	1E-6	87/04/20	2020	1E-5	88/10/09	0700	4E-23
85/06/12	1440	2E-6	87/04/21	1240	5E-6	88/10/12	1820	5E-5
85/06/13	0300	1E-5	87/05/06	1040	1E-4	88/10/13	1340	2E-5
85/06/16	0040	6E-5	87/05/22	1540	6E-5	88/10/14	1820	1E-6
85/06/19	0700	3E-6	87/05/24	1200	6E-5	88/10/14	2340	5E-5
85/06/20	0040	3E-5	87/05/27	0520	2E-5	88/10/21	0540	1E-23
85/06/22	0240	2E-5	87/05/21	0740	1E-6	88/10/27	0540	8E-5
85/06/23	0920	7E-5	87/05/21	1440	4E-6	88/10/29	2220	1E-5
85/06/25	1520	1E-5	87/05/30	1040	6E-5	88/11/28	1840	5E-5
85/07/04	0140	2E-6	87/05/30	1900	3E-5	88/11/29	0140	1E-5
85/07/09	0900	2E-5	87/06/01	0300	3E-5	88/11/30	2000	6E-9

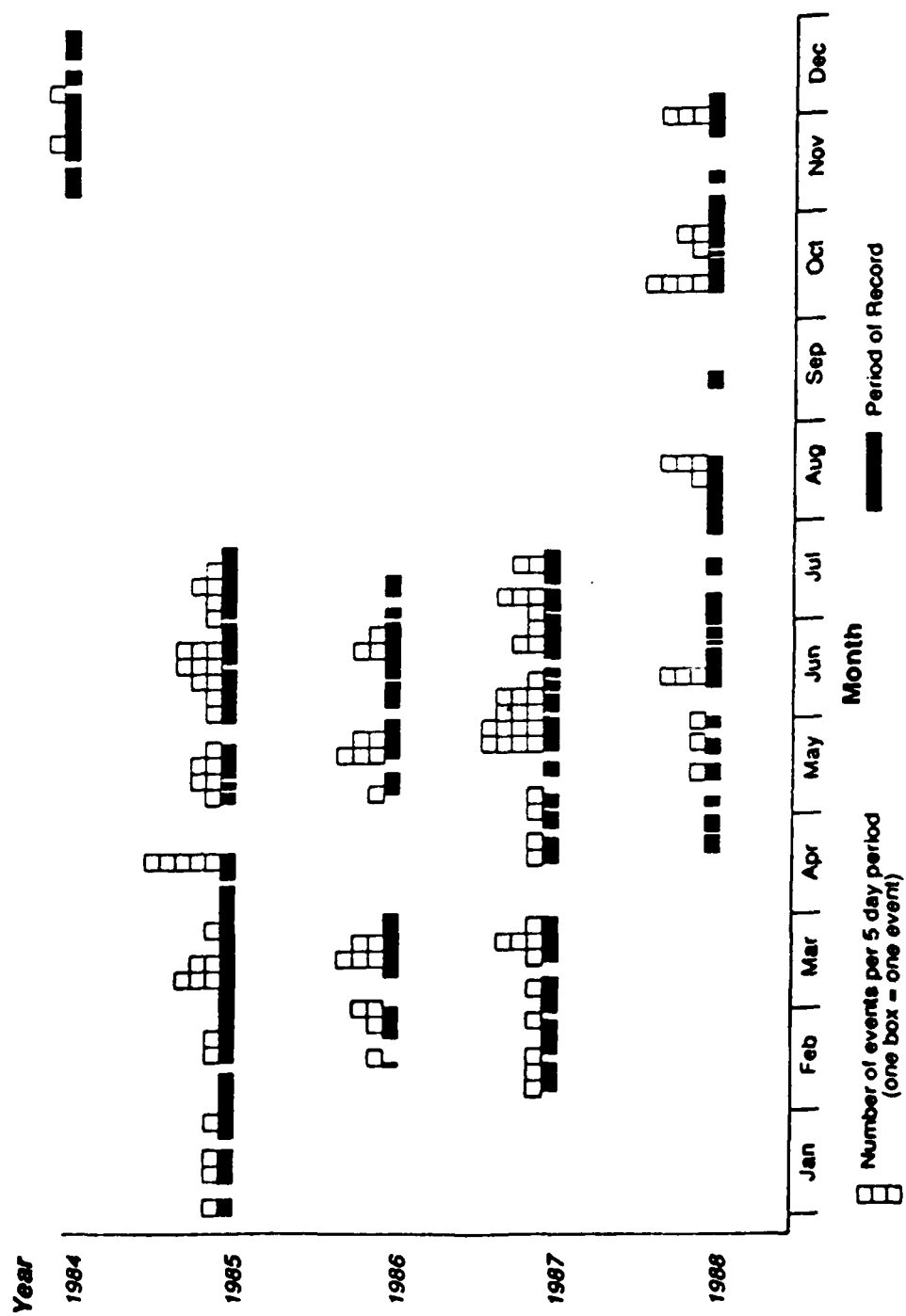


Figure 7.1: Low resolution event time line

1986, and 12-25 MAR 1986) indicate the data used in a similar study performed by Adams (1988).

7.2.2 High resolution time line

Figure 7.2 is a high resolution time line depicting the data set and several of its key characteristics. It was necessary to continue Figure 7.2 on several pages for the sake of readability. The broad dark horizontal lines illustrates the total period during which observations were being taken by the radiometer system for each month. Each box represents a 12-hour period of data. The markers protruding downward from the time line indicate that a 12-hour period was determined to be unusable for this study. The marker number gives the reason why the 12-hour period was omitted from the event search. If the average variance of a 12-hour period is too high it will be omitted from the search and assigned a marker number "2." Average variance relates to the signal-to-noise ratio and hence is a good measure of data quality.

When the 12-hour mean spectrum is very rough, it is unreliable for use in the search for events. Therefore, these 12-hour periods are not used in the search and are identified on Figure 7.2 by a number "3" marker. Similarly, if the 12-hour variance line is rough, it is not reliable in the event search. These 12-hour periods are given a marker

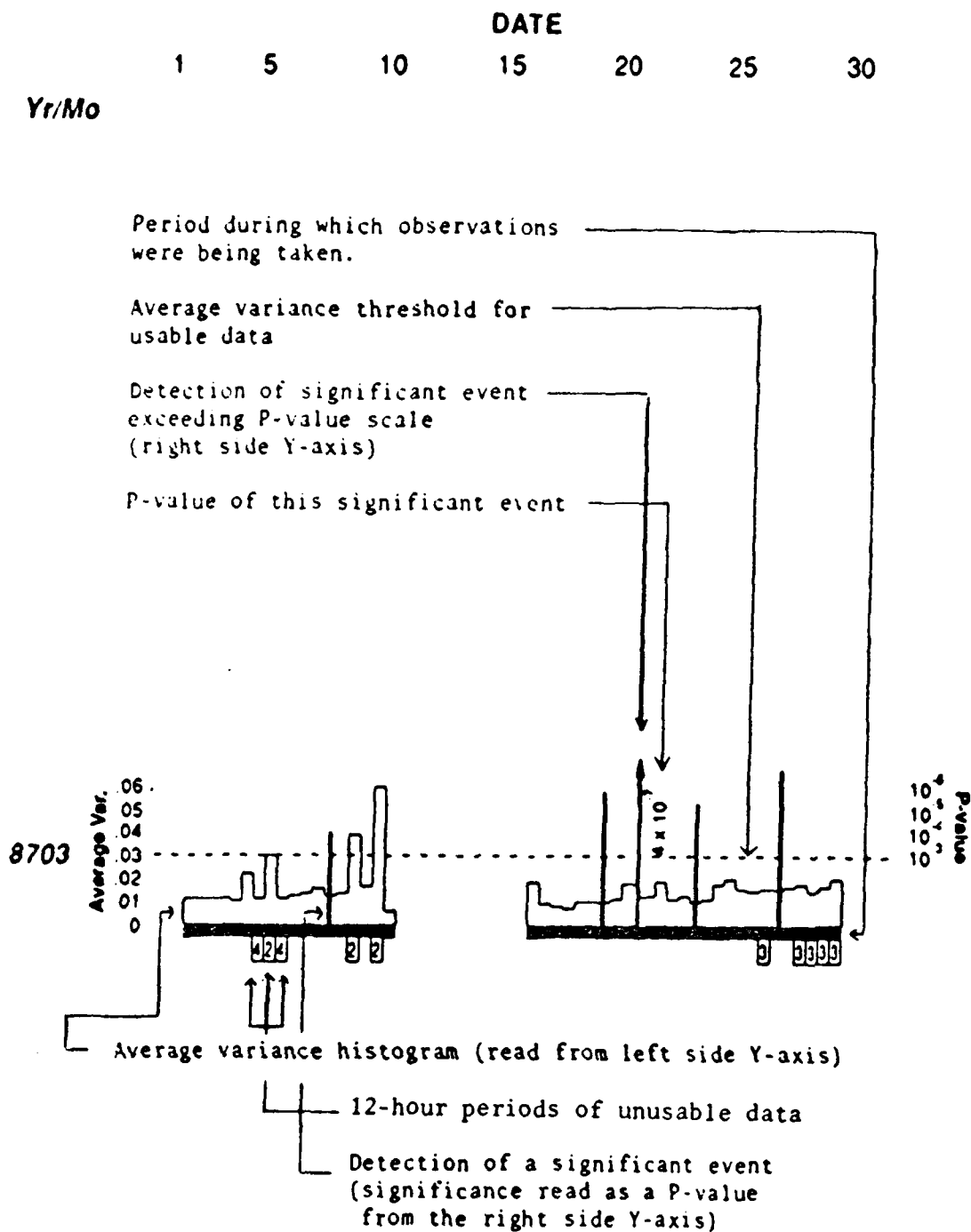


Figure 7.2: High resolution event time line. The first page displays the key for interpreting the following five pages.

(cont. on next page)

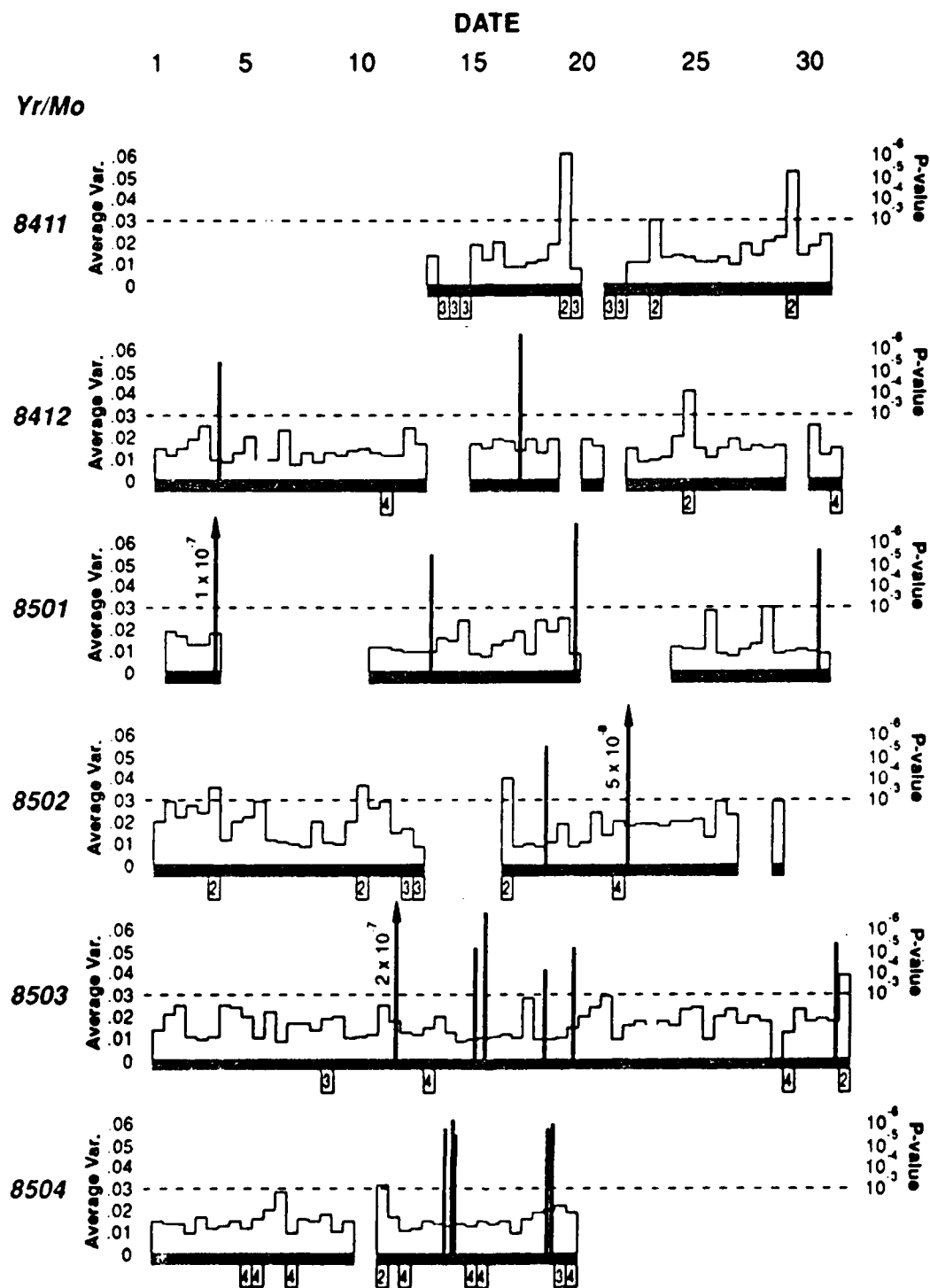


Figure 7.2: Continued

(cont. on next page)

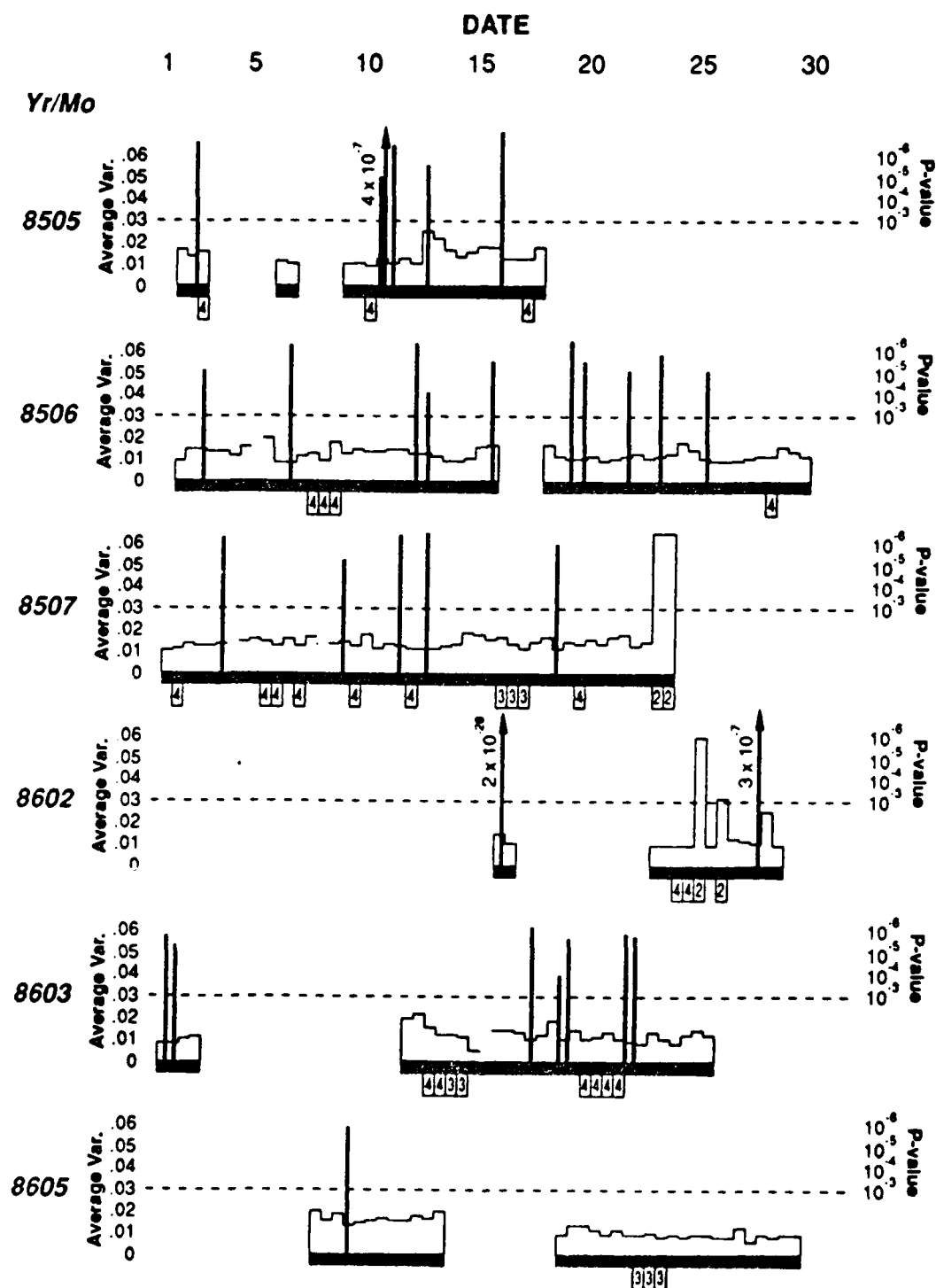


Figure 7.2: Continued

(cont. on next page)

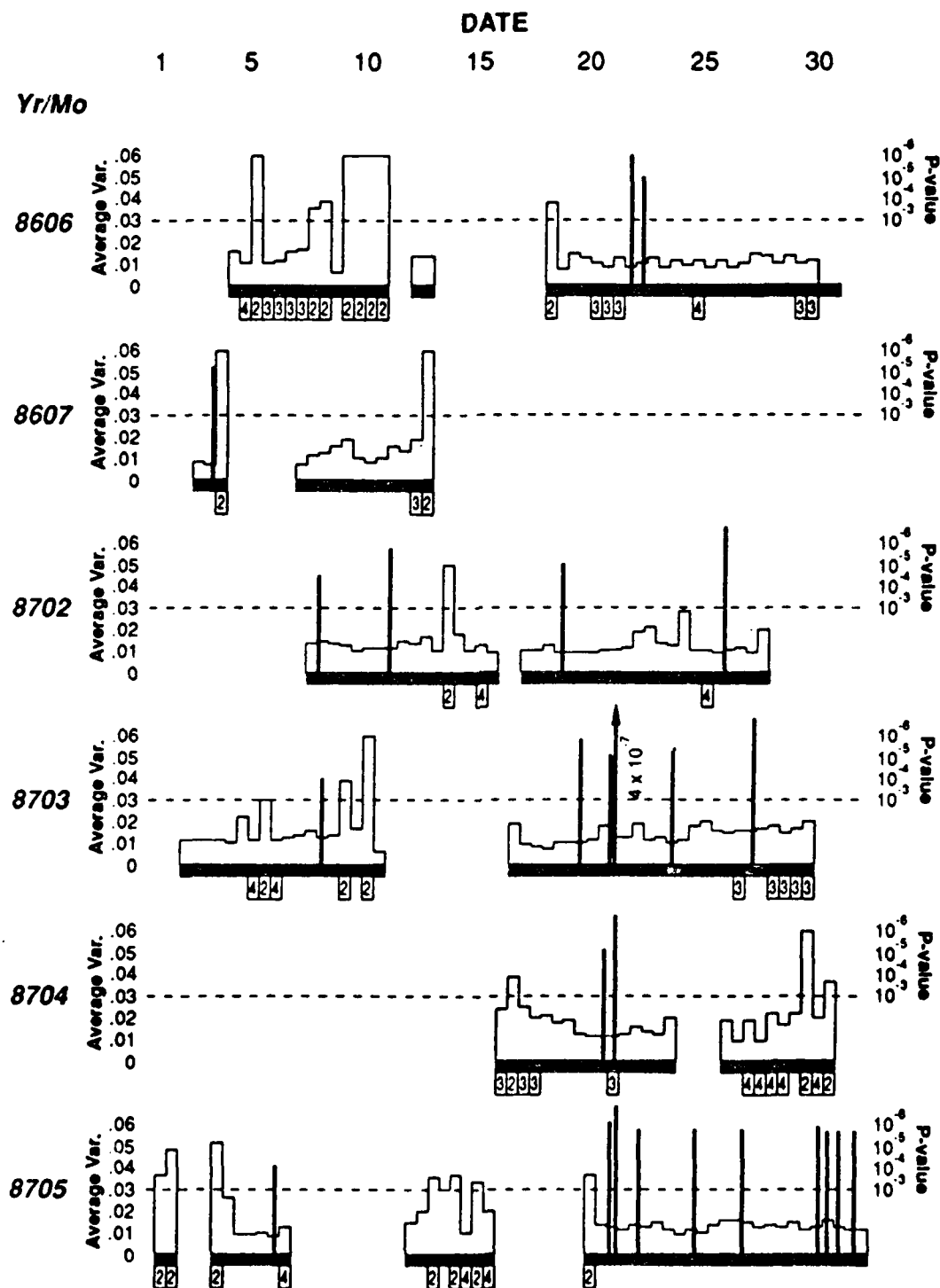


Figure 7.2: Continued

(cont. on next page)

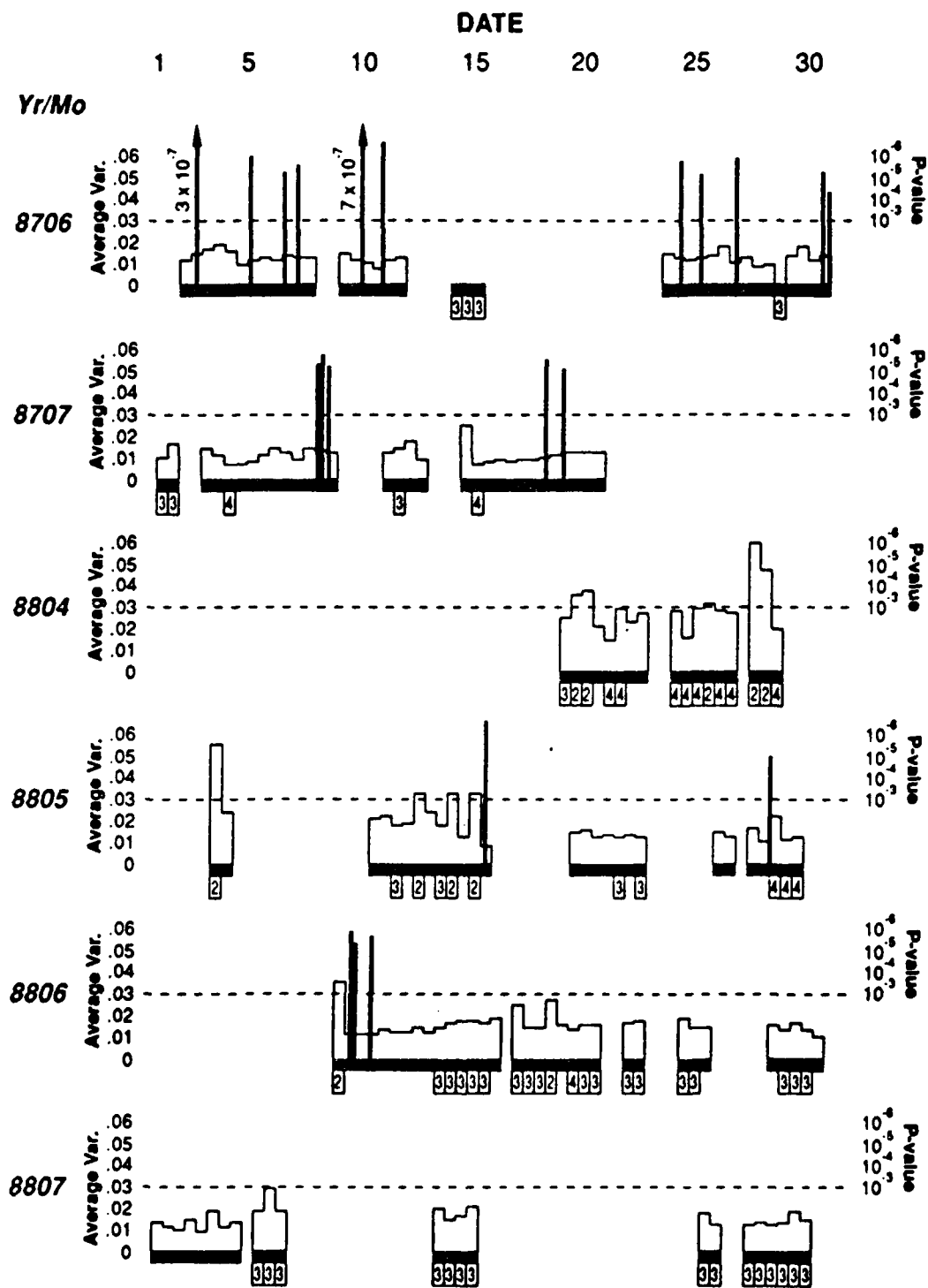


Figure 7.2: Continued

(cont. on next page)

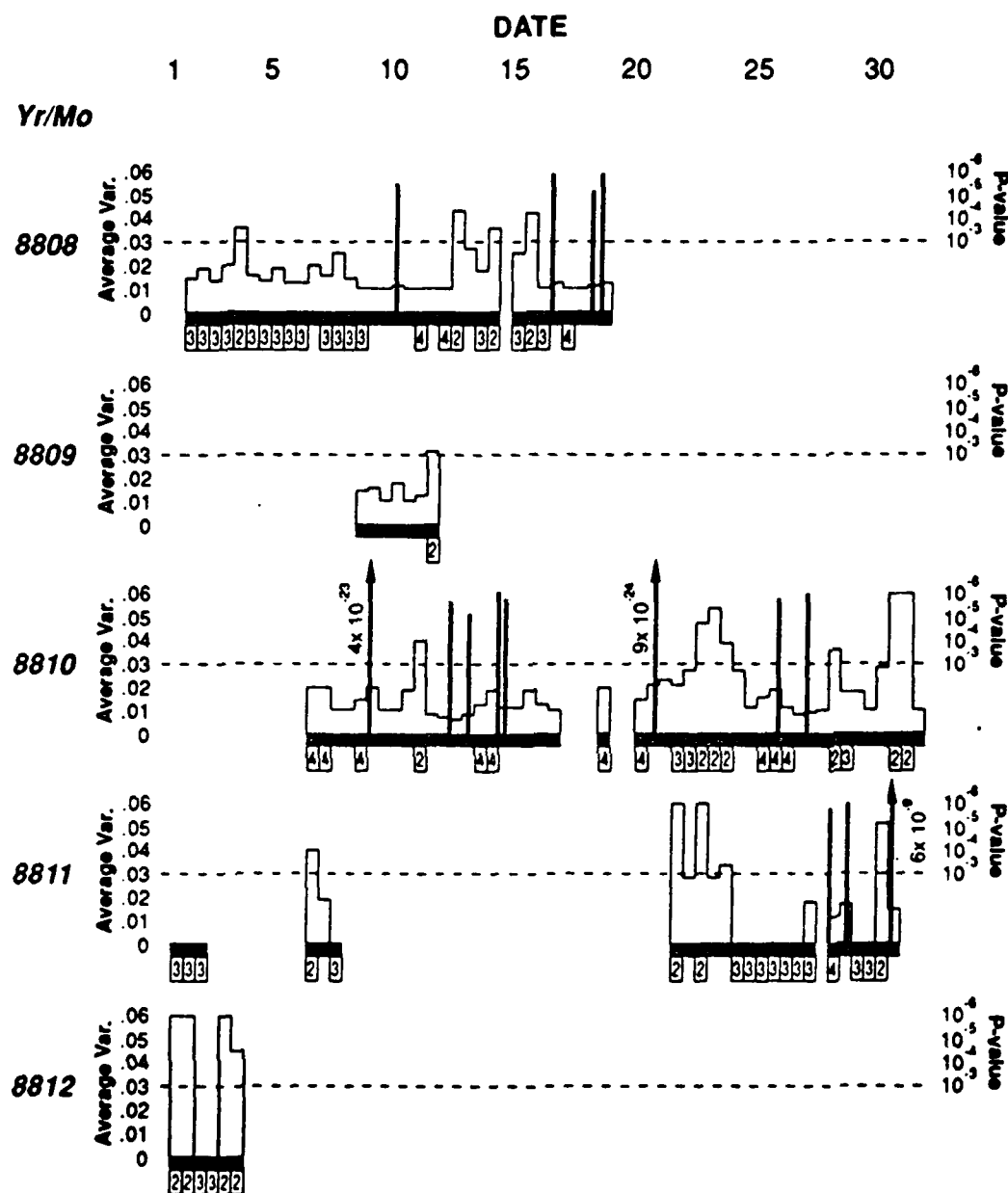


Figure 7.2: Continued

number "4" indicating that they have been omitted.

Note that the marker numbers relate to the test number in the data screening procedure described in section 5.3. This explains the absence of marker number "1" which relates to a test of 20-minute data rather than of 12-hour data.

The histogram refers to the average variance of the 12-hour period and is inversely related to the signal to noise ratio and hence data quality. The height of the histogram is measured by the left side, y-axis scale. The horizontal dashed line at $.03^{\circ}\text{K}$ is the average maximum variance for usable data.

The vertical lines indicate the events. Their horizontal positions on the monthly time line show the time of the occurrence. The line height, as measured by the right side y-axis scale, gives the P-value. If the event's P-value is less than 10^{-6} the line is topped with an arrowhead and the P-value is written along side the line.

Several interesting things can be seen from Figure 7.2. It is apparent that the occurrence of events is rather sporadic; however, they occasionally occur in clusters of two or three within 24 hours.

The data go through periods in which the average variance histogram is fairly smooth. These periods are indicative of good observing conditions (minimal tropospheric attenuation) and nominal equipment status. When the observing conditions are poorer or the equipment is

not performing well, the average variance histogram displays rough or spiked behavior

Clearly the nature of the data changed when the system was activated in April 1988. The number of 12-hour periods that were marked unusable became greater and the average variance histogram seemed to become more erratic with higher values. The explanation for this change is that during the data break from July 1987 to April 1988 the radiometer system was modified. A new wider bandwidth spectrometer was added to enable the system to gather data for lower altitudes. When the new spectrometer was brought on line the maser band width had to be widened at the expense of its amplifying power. As a consequence, the signal became weaker and the signal-to-noise ratio became smaller. This 10 to 20% decrease in signal to noise ratio would be sufficient to disturb the measurement of the mesospheric signal to the point at which the analysis algorithm would label the data unusable. (Note: For ordinary purposes, such as data inversion of the 12-hour or longer integrations, the data after April 1988 is still quite usable. The analysis procedure employed for this study was purposely chosen to maintain very stringent standards on data quality.)

7.2.3 Data statistics

Table 7.3 contains the year-by-year and total period statistics of the data set. The first row, labeled "Observation Days," gives the number of days on which data were collected. Listed in row 2, "Possible Observations," is the number of 20-minute observations that could have been taken if 72 observations were taken each day. The number of usable observations on record are listed in row 3, "Usable Observations." Row 4, "% Usable Data," gives the ratio of usable observations (row 3) to possible observations (row 2). These values, however, are not equal to one minus the percentage of data that was omitted, since row 2 contains the maximum number of observations that could be taken, not the actual number taken. Therefore, statistics based on row 2 data are lower limits rather than point estimators. The number of 20-minute observations meeting the criteria of the first screening for events are listed in row 5, "Possible Events." Row 6, "Significant Events," contain the number of observations meeting all the criteria for event detection. Row 7, "Days Between Significant Events," is calculated by dividing row 3 by 72 observations per day then dividing by row 6. The result can be expressed as the number of idealized days (72 consecutive 20-minute observations) between significant events. The time between events represents a lower limit. Row 8, "On-Air Days Between

Table 7.3: Summary of Event Statistics

	1984	1985	1986	1987	1988	Total
Observation Days	43	155	69	115	121	503
Possible Observations	3096	11160	4968	8280	8712	36216
Usable Observations	2467	8537	3306	5982	2540	22832
% Usable Data	79.7	76.5	66.5	72.2	29.2	63.0
Possible Events	8	120	33	115	33	236
Significant Events	2	38	13	38	20	111
Days Between Significant Events	17.13	3.10	3.53	2.19	1.76	2.86
On-Air Days Between Significant events	21.5	4.08	5.30	3.03	6.05	4.53

Significant Events," is obtained by dividing row 1 by row 6. It can be thought of as the average number of file days the algorithm had to search before finding an event. It is an estimate of the upper limit to the time between occurrences.

The results displayed in Table 7.3 highlight some interesting points. In row 4, "% Usable Data," the change in data character can easily be seen between the 1987 and 1988 statistics. This change to the system, explained in section 7.2.2, is not clearly seen in any other statistic.

An even more striking statistic appears in the 1984 column. The days between significant events are 5 to 6 times greater than other years. Here again, the data reflects a modification to the radiometer system. In February 1985, one of the local oscillators was replaced. The new part was later tested against the old part and proved to produce a more stable signal. The effect of the modification was to lower the system signal variance, thus making small comet detection easier. This effect can also be seen in the average variance histogram on Figure 7.2 between the months of February and March 1985. The monthly statistics (not reported) also reflect the change.

The most important statistic on Table 7.3 appears in the "Total" column. The upper and lower limits to the days between significant events were found to be around 4.5 days and 3 days. This compares favorably with the results reported by Adams (1988) which states that events were

detected about once every four days. Furthermore Adams reports that, based on model results and the geometry of the radiometer detection system, a small comet would traverse the radiometer beam about once every $1.5 \pm .3$ days depending on the assumption made about the altitude of detection. If one assumes that the capability to detect the water vapor from a small comet is less than 100%, their model results quickly approach the findings of both this and the Adams study.

If the events were produced purely by chance an event would be expected to occur at a rate equal to the alpha level of the search procedure hypothesis test, 1.25×10^{-4} (see section 6.2). Thus, chance would be expected to produce fewer than 3 events from the 22,832 useable spectra.

7.2.4 Trend analysis

The identification of trends within the data themselves and/or in the analyzed results often lends insight into the nature of the phenomenon being studied. The results of the trend analysis for this study follow.

No noticeable relationship was found between: event P-value and month/season, event P-value and time of day, frequency of occurrence (F_0) and time of day, F_0 and year, or F_0 and sunrise/sunset.

A weak trend was found between event P-value over the entire data set. P-values became slightly larger (events were less outstanding) as time went on. If true, a possible interpretation would be that the radiometer became slightly less sensitive over the years. This could be attributed to the physical modification mentioned in section 7.2.2.

If the ratio of observations used to the observations scanned for compiling the long period integration block is calculated, a weak relationship seems to exist between this value and the event P-value. As the ratio of observations used to observations scanned decreased, the P-value of the detected event also tended to decrease (event appeared to be more extreme). The trend also seemed to flatten out when the ratio went below .5. A likely explanation for this is that as the algorithm increases its scanning beyond 36 observations, because it encountered unusable 20-minute observations, it may be accepting data that are less similar to the suspect spectrum. Although this will tend to increase the variances of the center channels, it might also drive the long period average downward (if the long period average is increased, the chance of detection decreases, therefore limiting the balancing effect). When the ratio goes below .5, the number of observations used decreases, therefore increasing the variance by the central limit theorem (see section 6.2) and moderating the effect.

A weak relationship existed between F_0 and season.

More events seemed to be detected in the summer months than in the winter months. This may suggest a correlation with seasonal meteor shower cycles, but this relationship is beyond the scope of this study.

An interesting relationship seemed to exist between event P-value and F_0 . At the 95% confidence level the decrease in F_0 with P-value did not follow a normal distribution. This further supports the idea that the events are not caused by chance.

Finally, although no relationship appeared between antenna angle and event P-value or F_0 , an interesting anomaly appeared in the results. All three extreme outliers (Feb. 16, 1986, 17:20L; Oct. 9, 1988, 07:00L and Oct. 21, 1988, 05:40L) were detected at 15° antenna angle. Furthermore only 2,232 observations were taken at 15°, fewer than any other angle. These odd events could have been caused by read/write errors in the radiometer's minicomputer. It is conceivable that power surges could have caused a scaling exponent to be mishandled. This would have increased the channel values evenly across the spectrum. Records show that maintenance was being conducted about the time of the three events. Additionally, the event at 17:20L on February 16, 1986 occurred within 12 hours of system restart after a 7 month hiatus. Read/write errors affecting values other than the scaling exponent would have been caught and accounted for by the quality control

subroutine of the analysis software.

7.3 Selected case studies

For the purpose of familiarizing the reader with the emission spectra of event observations, three such spectra are presented in this section. These three spectra were carefully selected from the population of 111 events to illustrate three sub-classes of events, demonstrating varying degrees of uniqueness (based on P-value).

The 20-minute observation at 18:00L on March 18, 1985 (Figure 7.3) represents the marginal case for event detection. The P-value for this spectrum was calculated to be 1.21×10^{-4} , surpassing the detection threshold value 1.25×10^{-4} by only 4.0×10^{-6} . No other event was closer to this threshold value. In addition to its near threshold P-value, the folded observation is very smooth and well shaped. The "1st standard deviation" line is very close to the mean. Also, "36-period mean" line is extremely smooth. These parameters are indicative of very good observing conditions and a very high signal to noise ratio.

The second case study (Figure 7.4) illustrates the other extreme. It has one of the smallest (most unique) P-values of all the events, 1.96×10^{-7} (outliers excepted). In this case, the "36 period mean" spectrum is a relatively weak, noisy line with a standard deviation line which is

Case Study

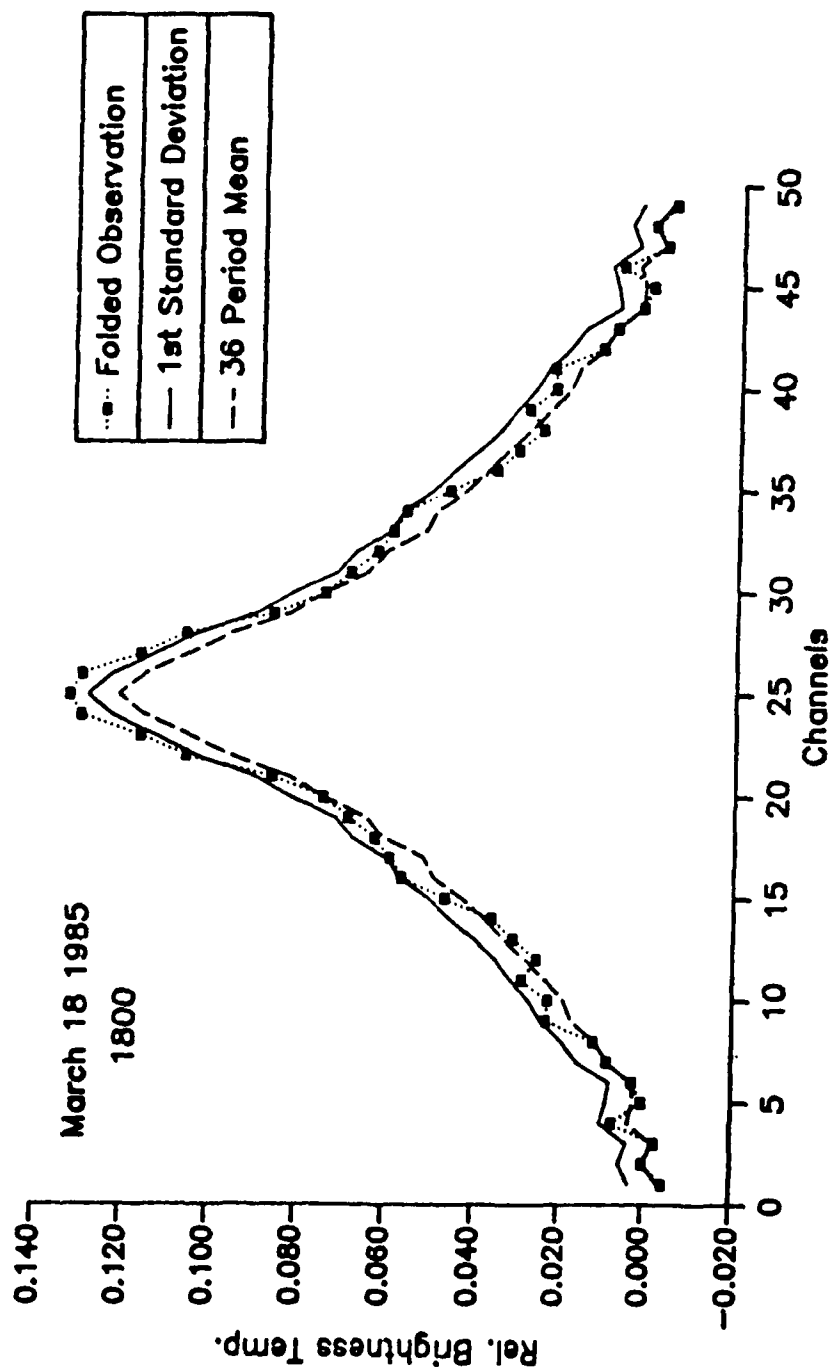


Figure 7.3: Case study of a near threshold P-value event spectrum. Relative brightness temperatures are not scaled to the system gain. Actual values would be 2 to 4 times greater.

Case Study

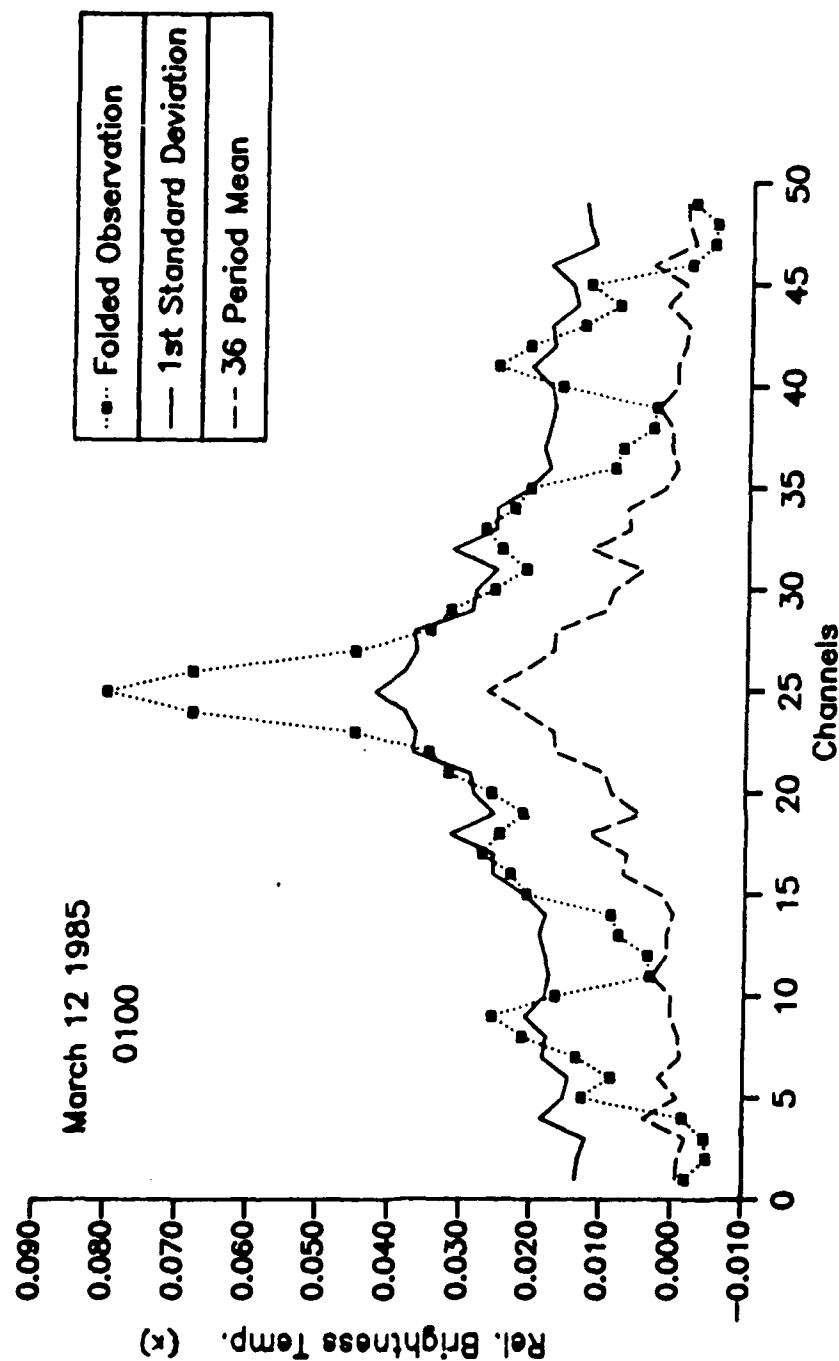


Figure 7.4: Case study of an extremely small P-value event spectrum. Relative brightness temperatures are not scaled to the system gain. Actual values would be 2 to 4 times greater.

relatively high. The folded observation line in this figure, is noise dominated on the wings, but is still rather smooth in the center. From this, one could infer fairly high tropospheric attenuation, yet a strong upper mesospheric/thermospheric signal.

The third case study event was chosen to be the observation at 03:20L on March 18, 1986. It was selected mainly because it was one of the events detected by Adams (1988). The benefit of selecting one of the events examined by Adams is that a crude data inversion of the spectra data was performed, thus we have an estimated vertical water vapor profile of a more or less typical 20-minute event observation to examine. The event spectrum (Figure 7.5) shows a fairly routine character with the exception of the center three channels which all have the same value and an unusual bulge on the wing between channels 13 and 20. The flat top is visually peculiar but easily explainable by chance of having the average of channels 24 and 26 in the unfolded spectrum equalling the value of channel 25. The bulge on the wing has defied physical explanation. Further consideration to "wing events," like this bulge, is given in section 7.4.

Figure 7.6 (adapted from Adams 1988) is the estimated vertical H_2O profile produced from the 03:20L observation on March 18, 1986. A large amount of smoothing was performed on the data in order perform the inversion. The profile is

Case Study

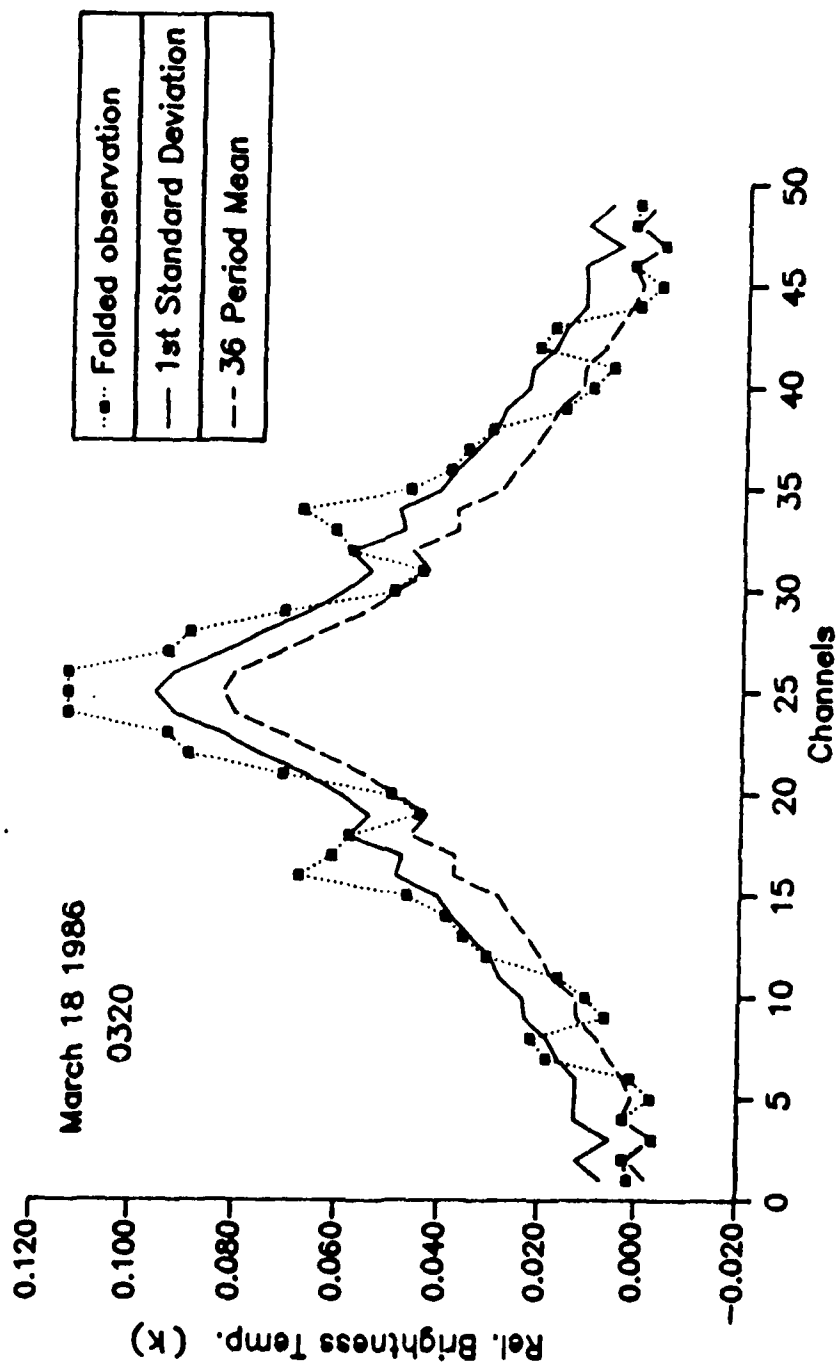


Figure 7.5: Case study of a typical event spectrum. Relative brightness temperatures are not scaled to the system gain. Actual values would be 2 to 4 times greater.

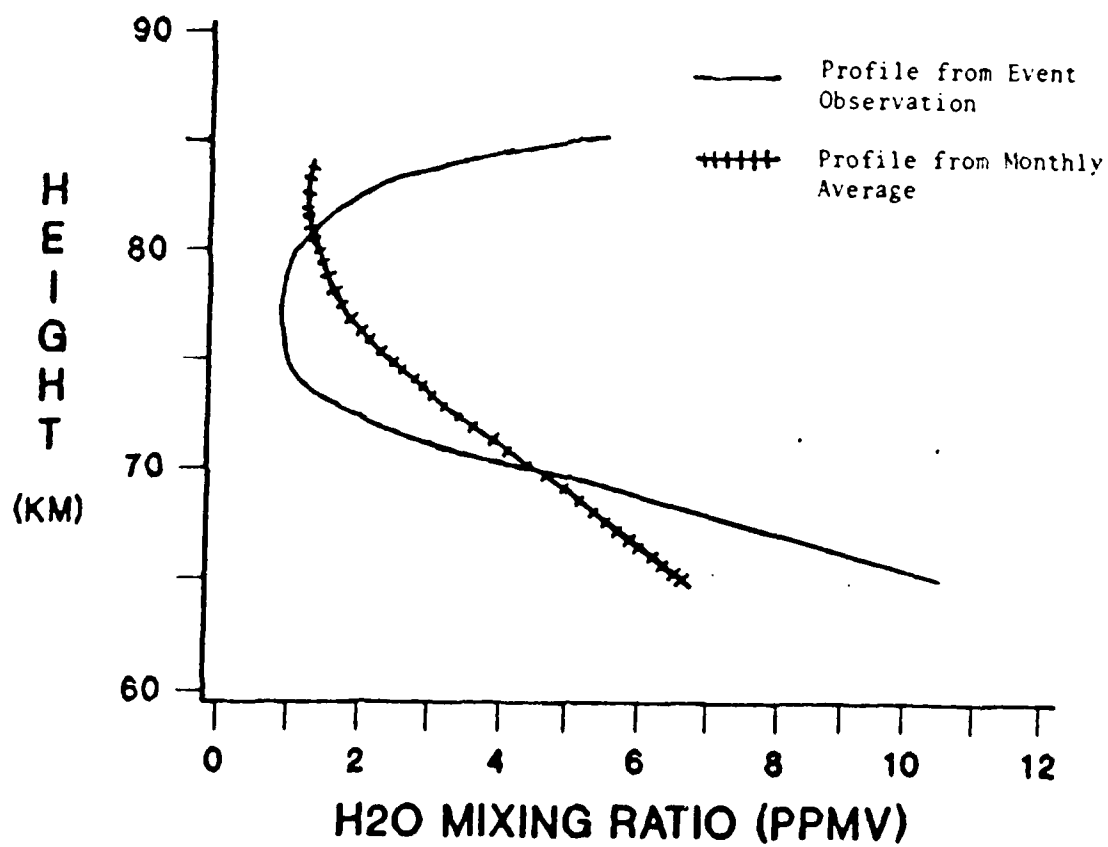


Figure 7.6: Vertical water vapor mixing ratio profiles for the event at 0320L on 18 March 1986. (Adams, 1988)

rather suspect due to the relatively low signal to noise ratio of this particular spectrum (and 20-minute spectra in general).

Two points to notice in Figure 7.6 are the extremely dry mesopause region and the sharp increase in water vapor above 80 km. Three of the four events identified by Adams (1988) produced profiles similar to this. Using these water vapor profiles he estimated that about 1×10^{30} water molecules had been added to the radiometer beam during each event. The monthly average vertical water vapor profile (Bevilacqua et al. 1989b) for March 1986 is also shown in Figure 7.6 for comparison.

7.4 Examination of spectral wings

The frequency of occurrence of events is much greater than that which is expected by chance. One possible explanation for such a high detection rate is local interference. In order to examine this possible source, the following hypothesis was proposed: an extraneous noise source or local interference could produce the signature of an event. If the interference affected the entire spectrum it would not be detected as an event. If the interference affected less than the entire spectrum it could be centered on the center channel and produce a false detection. Also, in order to defeat the rapid adjustments of the Dicke switching technique, the interference would have to be of a

short duration (less than one second). The final, and most important, consideration is that such a source would be equally as likely to be centered on any channel.

With this in mind, a test was designed to detect cases where the event signature was found in channels other than the center channel. A random period was selected and tested for normality (see section 6.2). Thirty-nine days from the months of May 1985 and June 1986 were used in this test. These periods yielded 2232 usable observation.

Four detection zones were examined: channels 4 to 6, channels 11 to 13, channels 18 to 20, and channels 23 to 25. The results of this test are summarized in Table 7.4. Based upon these results a series of statistical hypothesis tests were performed to determine the relationships between the 4 zones and chance. The following statements summarize the conclusions of the hypothesis tests. Although chance plays a major role in the results of the wing test on channels 4 to 6 and channels 11 to 13, something else is causing the events at channels 18 to 20. The contribution of this source to the total number of events detected at channels 23 to 25 is statistically insignificant.

Further analysis showed that one of the events, at channels 18 to 20, may have been caused by an excess water vapor event in the lower mesosphere. The emission spectrum showed high relative brightness temperatures between channels 16 and 34. The observation failed to be identified

Table 7.4: Summary of Spectral Wing Analysis

Channel #'s	4 to 6	11 to 13	18 to 20	23 to 25
Observation Days	39	39	39	39
Possible Observations	2808	2808	2802	2802
Usable Observations	2232	2232	2232	2232
Possible Events	3	8	20	51
Significant Events	0	1	2	16
Significant Events/ Usable observations	0	4.48E-4	8.96E-4	7.17E-3

as an event because the increased value of channel 25 was not statistically significant. Although an excess water vapor event affecting the lower mesosphere should be detectable, high noise levels in the center channels could cause it to go undetected. A search for this unique situation was considered beyond the scope of this study.

If this observation is not regarded as a "wing event," we can say that chance played an important role in all the results on the wings, but played practically no role in the center events. In summary, local interference, noise or chance do not significantly contribute to the 111 events detected at line center.

7.5 Rocket water release experiment

In an experiment to test the small comet theory, another research group launched a series of rocket flights from the Wallops Island launch facility during the summer of 1988. The purpose of these flights were to recreate the atmospheric responses that would be caused by a small comet impact. The Dynamics Explorer satellite observed the disturbed area to determine whether an atmospheric hole was detectable. Sizable quantities of water were released into the thermosphere by these rocket flights. The rocket payloads consisted of 580 lbs of liquid water ($5-7 \times 10^{27}$ H_2O molecules) which vaporized or froze upon release into the

upper atmosphere. These releases created strong localized interaction with the ionosphere due primarily to cluster ion recombination. This was detected by the Dynamics Explorer satellite as a spherical hole (100 km in diameter) in the Earth's atomic oxygen dayglow imagery. The duration of this disturbance was only a few minutes.

On the third, and final launch, the payload was released at 300 km altitude at 37.6°N latitude, 74.2°W longitude at 17:00 Zulu time on September 10, 1988. Prior to the release period the Penn State microwave radiometer was adjusted to view the release point. During the release period, observations were taken every 5 minutes. These 5-minute spectra were not analyzed when the routine search procedure was conducted on the September 88 data. No events were detected among the 288 20-minute observations taken between September 8 and 11, 1988.

When a special analysis of the 5-minute data was performed, it was found to have a signal-to-noise ratio that was too low for reliable use. These 5-minute observations were then added to form 20-minute periods during which no events were detected. A significant increase of water vapor was observed three hours after the release time. This increase lasted for several hours, but still did not reach the event detection threshold.

In order for the radiometer to sense water, the water molecules must be in the vapor state and in the lowest

energy state. It is likely that many of the rocket delivered water molecules froze as they were released into the thermosphere. The water molecules may also have undergone higher energetic transformations in the presence of the solar radiation. Due to the very large mean free paths at 300 km, it could have taken several hours to thermalize these energetic molecules. It also would take time for any ice crystals to sublimate to the vapor state. The appearance of the increase in water vapor at the launch + 3 hours point, may or may not have been caused by the water released during the experiments.

7.6 Possible causes of events

Having eliminated chance, local interference, and noise as the primary cause for the events, it is necessary to discuss other possible causes.

Possible geophysical explanations can be grouped into two categories: 1. perturbations of the mesospheric/thermospheric water vapor and 2. perturbations of the mesospheric/thermospheric temperature within the radiometer's volume of detection. Since detected events never occurred on consecutive 20-minute periods the increase and decline of water vapor or temperature must be a very short-lived disturbance. If we assume a symmetric increase and decline of the perturbed parameter (because this

represents the smallest time rate of change) then the duration of the disturbance should be less than 20 minutes. This also assumes that adjacent 20-minute observations are affected by the perturbation but not beyond the threshold level for event detection. This places a severe time constraint on any disturbance responsible for an event.

Several phenomena could cause a disturbance in the water vapor concentration. Chemical reactions involving methane or odd hydrogen and dynamic effects such as vertical advection and turbulent mixing were examined by Adams (1988) as possible causes of the detected events. He concluded that none of these mechanisms were capable of producing the necessary perturbation required for event detection.

Temperature anomalies which could possibly produce an event could be caused by gravity waves, solar flares, or geomagnetic disturbances. If we assume an average vertical water vapor distribution, the temperature perturbation capable of being detected by the radiometer would have to be confined to the atmosphere below about 100 km. This statement is made because so few water molecules reside above the 100 km level that very little contribution can be made to the total signal received by the radiometer from higher altitudes.

The amplitude of a temperature anomaly capable of producing an event can be estimated by considering the threshold values for an event and equation 4.3. Typically,

the 1.5 standard deviation level is about 10% greater than the mean value of the center channels of the spectrum. Since this is 10% of the "relative" brightness temperature rather than the "absolute" brightness temperature, all contribution from the atmosphere below around 40 km is removed from consideration due to pressure broadening. Thus the integral term of equation 4.3 evaluated from 40 km to 100 km must undergo a 10% perturbation within a 20-minute period. An annual average temperature for that layer of the atmosphere should be between 210°K and 230°K which yields a perturbation amplitude near 22°K.

One possible cause of event detection might be the temperature perturbation of propagating gravity waves. The temperature perturbation of gravity waves travelling through the mesosphere have been observed to be as great as 30°K (Fritts 1984). The vertical wavelength of gravity waves carrying large temperature perturbations is usually between 2 - 20 km with phase speeds of less than 30 m s⁻¹ (Schoeberl et al. 1981). Gravity waves can be generated by a number of sources including intense tropospheric convection, terrain forcing, geomagnetic storms, and solar flares. If the axis of the radiometer beam is nearly parallel to the wave fronts of the gravity wave, the average temperature of the volume observed by the radiometer could be affected. Without this orientation, the atmosphere along the optical path of the radiometer would experience

alternating zones of heating and cooling. This would not produce a significant increase in the integrated temperature of the atmosphere along the radiometer's optical path. If we assume that the wave is aligned parallel to the beam, the integrated temperature would rise and fall with the passage of the wave. Since gravity waves usually consist of more than one period, several temperature oscillations would occur over the course of time. It is possible an event would be registered if the wave speed is such that one 20-minute observation is taken during the heating phase and the next observation is taken during the cooling phase. If waves of a greater speed are encountered, alternating periods of heating and cooling within the same 20-minute observation would result. In this case, an event would not be likely to register. If the phase speed is too slow, consecutive 20-minute observations would be affected by each phase. Results in this study show that there were no cases in which events were detected in consecutive 20-minute observations. Even if the wave's speed and orientation are ideal, events could be recorded a maximum of every other 20-minute observation. This is not a characteristic of the event distribution.

Gravity wave breaking is known to deposit thermal energy into the mesosphere (Fritts 1984). It is conceivable that a localized area being observed by the radiometer could receive enough thermal energy to cause an increase in the

received signal. Calculations based on in situ measurements taken between 55 km and 70 km have revealed that the mesosphere can be heated by gravity wave breaking at rates as great as $400^{\circ}\text{K}/\text{day}$ (2.8°K per 10 minutes) (Taylor 1979). Intense tropospheric convection was found to be the source of these gravity waves. The increases in temperature, however, are not quickly dissipated (Dickinson 1984) and thus, cannot produce an event detection. Furthermore, in the northeastern United states, the frequency of intense convection is far less than that of the occurrence of events. This is especially true in the winter.

Sudden intensification of solar radiation is also a possible candidate for providing a false water vapor measurement. Solar flares are quite capable of causing very large and rapid increases in the thermospheric temperature. The increase in EUV radiation accompanying a solar flare theoretically could cause mesospheric temperatures to increase tens of degrees (Geller 1981). However, Newtonian cooling rates are far too slow to dissipate this thermal energy within the time constraints (Kiehl and Solomon 1986). Without a strong cooling mechanism, solar flares can not be considered a viable explanation for the detected events.

Geomagnetic disturbances could cause sudden changes in the ionosphere and auroral activity which, in turn, leads to increased joule heating of the atmosphere. Ramakrishna and Seshamani (1973; 1976) determined that disturbances in the

geomagnetic field can cause rapid fluctuations in the mesosphere (60 km - 90 km) in the vicinity of the auroral and equatorial electrojets of as much as 9°K. Roble et. al. (1987) point out that joule heating elsewhere in the mesosphere could only produce a heating rate of 1°K - 3°K per day, far less than what is needed for event generation.

Although these explanations, along with the read/write error scenario which might account for the three outliers among the events, described in section 7.2.4, deserve consideration, it seems unlikely that they are responsible for the events reported in this study.

The small comet hypothesis provides the only remaining explanation for the detected events. This is not surprising, since the detection procedure was designed to identify those observations which displayed the characteristics we would expect to see generated by a small comet impact. The fact that only one viable explanation exists to explain the number of detections further strengthens the evidence in support of the small comet theory.

Chapter 8

SUMMARY, CONCLUSIONS, AND RECOMMENDATIONS FOR FUTURE WORK

8.1 Summary

A search for extremely large transient increases in the concentrations of mesospheric/thermospheric water vapor was conducted as part of this study. Data for the analysis were obtained using a ground-based microwave radiometer located at Penn State. More than 22,000 observations, recorded on 503 days during the period of November 1984 to December 1988, were used in the search. This procedure was performed to provide information concerning a proposed extraterrestrial water vapor source for the upper atmosphere. Also, a statistical analysis was completed using the results from this study. Finally, alternative explanations were examined to ascertain if they could be the cause of the detected events. An analysis of one of these explanations involved the search for possible positive anomalies on the wings of the water vapor spectral observations. This analysis was performed to determine if the signature defined as an event was unique to the spectral line center.

8.2 Conclusions

Following are the primary conclusions that can be made based upon this project:

- An alternate hypothesis which assumed that anomalies are equally likely to occur on the spectral wings has been disproven. Therefore, the events at line center can not be attributed to interference, instrument error, or chance.

- Positive thermal anomalies of the mesosphere/thermosphere which might cause event detection, occur too infrequently (if at all) to account for the events that were detected. Terrestrial temperature perturbations (e.g. waves) have significantly different temporal signatures.

- Recent work by Adams (1988) suggests that transient water vapor increases in the upper atmosphere have no plausible source other than the small comet hypothesis. We accept this conclusion.

- The event detection statistics presented in Table 7.3 give an upper and lower limit for the average detection rate. These limits are one event every 3 ± 1 days and one every 4.5 ± 1 days, respectively. These rates are far greater than those produced by chance. The detection rates are comparable to the findings of Adams (1988) who, using a much smaller sample size, reported, on average, an event occurring about once every four days. This rate also

compares favorably with a detection rate of one event about every two days estimated from the Frank-Sigworth-Craven (FSC) small comet theory.

- The FSC small comet theory provides the only remaining explanation for the events detected. Therefore, the results of this study support the FSC small comet theory.

8.3 Recommendations for future work

The data collected by the Penn State microwave radiometer are the best available for mesospheric water vapor. The data set is both semi-continuous and of relatively high temporal resolution. Presented below are suggestions for future work to be performed using this data base.

- The enhanced water vapor events reported in this study should be compared one to one with the appearances of atmospheric holes in the Dynamics Explorer satellite imagery. A strong correlation between these two phenomena would provide rather conclusive evidence for the small comet theory.

- The observations immediately following the bin containing each of the 111 events should be analyzed for residual cometary water vapor. The small comet influx model may require revision based on the results of this analysis.

- The 111 events spectra should be combined (superimposed) to produce a single average event spectrum. This spectrum could then be inverted to yield an average event vertical water vapor profile. This information could show us at what altitudes cometary water vapor is being deposited.

- The analysis software developed for this project could be modified to handle the wide band data which has been collected since April 1988. Since the criteria used for this study were very stringent, changes would have to be made in the data screening process. The new techniques for baseline removal would also have to be incorporated.

- A link should be established between the radiometer system's microcomputer and the mainframe at the Penn State Center for Academic Computing. This would make the latest data almost immediately accessible and would eliminate the labor involved in transferring data manually.

- A channel-by-channel analysis of the data set could be performed to find oscillations of various time scales. The 20-minute integrations should provide sufficient temporal resolution to detect atmospheric tidal waves (with periods of 6 to 24 hours) and, perhaps, gravity waves (with periods of 1 to 6 hours).

These suggestions would not only provide additional evidence concerning the controversial small comet theory,

but would also lead to greater insight into upper atmospheric processes effecting water vapor.

BIBLIOGRAPHY

- Adams, D.M. (1988): Extreme short-term variability in upper atmospheric water vapor as measured by ground based microwave radiometry, M.S. Thesis, The Pennsylvania State University, University Park, Pennsylvania.
- Allen, M., Y.L. Yung, and J.W. Waters (1981): Vertical transport and photochemistry in the terrestrial mesosphere and lower thermosphere (50-120 Km), Journ. of Geophys. Res., 86, 3617.
- Arnold, F., and D. Krankowsky (1977): Water vapour concentrations at the mesopause, Nature, 268, 218.
- Bevilacqua, R.M. (1982): An observational study of water vapor in the mid-latitude mesosphere, Phd. Thesis, The Pennsylvania State University, University Park, Pennsylvania.
- Bevilacqua, R.M., M. Allen, D.F. Strobel, M.E. Summers, and J.J. Olivero, (1989a): The seasonal variability of water vapor and ozone in the upper mesosphere: implications for vertical transport and ozone photochemistry, Manuscript submitted to the Journ. of Geophys. Res. (Atmospheres), Aug 1989.
- Bevilacqua, R.M., J.J. Olivero, and C.L. Croskey (1989b): Mesospheric water vapor measurements from Penn State: Monthly mean observations (1984 - 1987), Journ. of Geophys. Res., 94, 12807.
- Brasseur G., and S. Solomon (1984): Aeronomy of the Middle Atmosphere, D. Reidel Pub. Co., Dordrecht, Holland.
- Brewer, A.W. (1949): Evidence for a world circulation provided by the measurements of helium and water vapour distribution in the stratosphere, Quart. J. Roy. Meteor. Soc., 75, 351.
- Chubb, T.A. (1986): Comment on the paper "On the influx of small comets into the Earth's upper atmosphere I. Observations," Geophys. Res. Lett., 13, 1075.
- Cragin, B.L., W.B. Hanson, R.R. Hodges, and D. Zucarro (1986): On the influx of small comets into the Earth's upper atmosphere I. Observations, Geophys. Res. Lett., 14, 573.

- Davis, P.M. (1986): Comment on the paper "On the influx of small comets into the Earth's upper atmosphere," Geophys. Res. Lett., 13, 1181.
- Devore, J.L. (1987): Probability and Statistics for Engineering and the Sciences, 2d ed., Brooks/Cole Publishing Company, Montreal, Canada.
- Dicke, R.H. (1946): The measurement of thermal radiation at microwave frequencies, Rev. Sci. Instr., 17, 268.
- Dickinson, R.E. (1984): Infared Radiative Cooling in the Mesosphere and Lower Thermosphere, Journ. of Atmos. Terr. Phys., 46, 995.
- Dobson, G.M.B., A.W. Brewer, and B.M. Cwilog (1946): Meteorology of the lower stratosphere, Proc. Roy. Soc., London, A185, 144.
- Donahue, T.M. (1986): Comment on the paper "On the influx of small comets into the Earth's upper atmosphere II. Interpretation," Geophys. Res. Lett., 13, 557.
- Donahue, T.M., T.I. Gombosi, and B.R. Sandel (1987): Cometasmals in the inner solar system, Nature, vol 330, 584.
- Fedynski, A.V., and V.A. Yushkov (1980): Direct measurements of water vapor concentraions in the stratosphere and mesosphere in the mid-latitudes of the USSR and in the equatorial zone, in Low Altitude Aeronomical Processes, COSPAR Advances in Space Exploration, A.P. Mitra Ed., 8, Permagon, 263.
- Frank, L.A. (1989): Atmospheric holes and the small comet hypothesis, Australian Physicist, 26, 19.
- Frank L.A., J.D. Craven, K.L. Ackerson, M.R. English, R.H. Eather, and R.L. Carovilla (1981): Global auroral imaging instrumentation for the Dynamics Explorer mission, Space Sci. Instr., 5, 369.
- Frank L.A., J.B. Sigworth, and J.D. Craven (1986a): On the Influx of small comets into the Earth's upper atmosphere, I. Observations, Geophys. Res. Lett., 13, 303.
- Frank L.A., J.B. Sigworth, and J.D. Craven (1986b): On the Influx of small comets into the Earth's upper atmosphere, II. Interpretation, Geophys. Res. Lett., 13, 307.

- Frank L.A., J.B. Sigworth, and J.D. Craven (1986c): Reply to Donahue, Geophys. Res. Lett., 13, 559.
- Frank L.A., J.B. Sigworth, and J.D. Craven (1986d): Reply to Hanson, Geophys. Res. Lett., 13, 985.
- Frank L.A., J.B. Sigworth, and J.D. Craven (1986e): Reply to Chubb, Geophys. Res. Lett., 13, 1079.
- Frank L.A., J.B. Sigworth, and J.D. Craven (1986f): Reply to Davis and Nakamura, et al., Geophys. Res. Lett., 13, 1186.
- Frank L.A., J.B. Sigworth, and J.D. Craven (1986g): Reply to Rubincam, Geophys. Res. Lett., 13, 703.
- Frank L.A., J.B. Sigworth, and J.D. Craven (1986h): Reply to Morris, Geophys. Res. Lett., 13, 1484.
- Frank L.A., J.B. Sigworth, and J.D. Craven (1986i): Reply to McKay, Geophys. Res. Lett., 13, 979.
- Frank L.A., J.B. Sigworth, and J.D. Craven (1986j): Reply to Soter, Geophys. Res. Lett., 14, 164.
- Frank L.A., J.B. Sigworth, and J.D. Craven (1987a): An atomic hydrogen torus around the sun from a large population of small comets, Univ. of Iowa Res. Rep. 88-9, 1989.
- Frank L.A., J.B. Sigworth, and J.D. Craven (1987b): Reply to Cragin et al., Geophys. Res. Lett., 14, 577.
- Frank L.A., J.B. Sigworth, and J.D. Craven (1987c): Reply to Wasson and Kyte, Geophys. Res. Lett., 14, 781.
- Frank L.A., J.B. Sigworth, and J.D. Craven (1987d): A hypothesis concerning the inner Oort disk and its relation to comet showers and extinction of species, paper presented to the American Astronomical Society Nov. 1987.
- Fritts, D.C. (1984): Gravity wave saturation in the middle atmosphere: a review of theory and observations, Rev. of Geophys. and Space Phys., 22, 275.
- Geller, M.A. (1981): Planetary wave coupling between the troposphere and the middle atmosphere as a possible sun-weather mechanism, in "Summary Report of Studies as a Search for Physical Mechanisms Relating Solar Variability and the Troposphere," S.T. Wu Ed., NASA CR-161762, 45.

- Girard, A., J. Besson, D. Braird, J. Laurent, M.P. Lemaitre, C. Lippens, C. Muller, J. Vercheval, and M. Ackerman (1988): Global results of GRILLE spectrometer experiment on board Spacelab 1, Planet. Space Sci., 36, 291.
- Hanson W. (1986): Comment on the letter "On the influx of small comets into the Earth's upper atmosphere II. Interpretations," Geophys. Res. Lett., 13, 981.
- Hunt, B.G. (1966): Photochemistry of ozone in the moist atmosphere, Journ. of Geophys. Res., 71, 1385.
- Huyghe, P., (1988): Oceans from comets - New evidence, Oceans, 21, 2 March-April, 1988, 8.
- Jursa, A.S., Ed. Handbook of Geophysics and the Space Environment, Air Force Geophysics Laboratory, 1985.
- Kerr, A.R., (1987): In search of elusive little comets, Science, 240, 1404.
- Kiehl, J.T., and S. Solomon (1986): On the Radiative Balance of the Stratosphere, Journ. of the Atmos. Sci., 43, 1525.
- Kunzi, K.F., E. Lobsiger, and G.K. Hartmann (1983): Water vapor measured in the middle atmosphere with an airborne microwave radiometer, Six ESA Symposium on European Rocket and Balloon Programmes, (ESA SP-183), 173.
- Le Texier, H., S. Solomon, and R.R. Garcia (1988): The role of molecular hydrogen and methane oxidation in the water vapor budget of the stratosphere Quart. J. Roy. Meteor. Soc., 114, 281.
- Liou, K.N. (1980): An Introduction to Atmospheric Radiation, Academic Press Inc., New York, NY
- Longbothum, R.L. (1976): A Study of Water Vapor Measurements in the Stratosphere and Mesosphere Using Microwave Techniques, Scientific Report 449, (PSU-IRL-SCI-449), Ionospheric Research Laboratory, The Pennsylvania State University, University Park, PA.
- McKay, C.P. (1986): Comment on the paper "On the influx of small comets into the Earth's upper atmosphere II. Interpretation," Geophys. Res. Lett., 13, 976.

- Miller, I., and J.E. Freund (1977): Probability and Statistics for Engineers, Prentice-Hall Inc., Englewood Cliffs, NJ.
- Morris, D.E. (1986): Comment on "On the influx of small comets into the Earth's upper atmosphere II. Interpretations," Geophys. Res. Lett., 13, 1482.
- Murgatroyd, R.J. (1969): in The Global Circulation of the Atmosphere, G. A. Corby Ed., Roy. Met. Soc., (London).
- Nyquist, H. (1928): Thermal agitation of electric charge in conductors, Phy. Rev., 32, 110.
- Olivero, J.J., and R.M. Bevilacqua (1989): AMS meeting on the middle atmosphere, San Francisco, CA, April 1989.
- Peter, R., K. Kunzi, and G.K. Hartmann (1988): Latitudinal survey of water vapor in the middle atmosphere using an airborne millimeter wave sensor, Geophys. Res. Lett., 15, 1173.
- Radford, H.E., M.M. Litvak, C.A. Gottlieb, E.W. Gottlieb, S.K. Rosenthal, and A.E. Lilly (1977): Mesospheric water vapor measured from ground-based microwave observation, Journ. of Geophys. Res., 82, 472.
- Ramakrishna S., and R. Seshamani (1973): The effect of solar activity on temperature in the equatorial mesosphere, Journ. of Atmos. Terr. Phys., 35, 1631.
- Ramakrishna S., and R. Seshamani (1976): Day-night dependence of geomagnetic activity effects on mesospheric temperatures, Journ. of Geophys. Res., 81, 6173.
- Reid, G.C., and S. Solomon (1986): On the existence of an extraterrestrial source of water vapor in the middle atmosphere, Geophys. Res. Lett., 13, 1129.
- Remsberg, E.E., J.M. Russell III, L.L. Gordley, J.C. Grille, and P.L. Bailey (1984): Implications of stratospheric water vapor distributions as described from the Nimbus 7 LIMS experiment, Journ. of the Atmos. Science, 41, 2934.
- Roble, R.G. (1987): Joule heating the mesosphere and thermosphere during the July 13, 1982 solar proton event, Journ. of Geophys. Res., 92, 6083.

- Schoeberl, R.M., D.F. Strobel, J.P. Apruzese (1983): A numerical model of gravity wave breaking and stress in the mesosphere, Journ. of Geophys. Res. (Atmos.), 88, 5249.
- Scholz, T.G., D.H. Ehhalt, L.E. Heidt, and E.A. Martell (1970): Water vapor, molecular hydrogen, methane and tritium concentrations near the stratopause, Journ. of Geophys. Res., 75, 3049.
- Soter, S., (1987): Comment on "On the influx of small comets into the Earth's upper atmosphere," Geophys. Res. Lett., 14, 162.
- Steinberg, J.L., and J. Lequeux (1963): Radio Astronomy, McGraw-Hill Book Co., New York, NY
- Stewart, A.I.F., B.M. Jakosky, G.R. Gladstone, and R.T. Clancy (1986): On the observation and analysis of atmospheric holes observed by Dynamics Explorer 1, Preprint.
- Taylor, L.L. (1979): Mesospheric Heating due to Intense Tropical Convection, NASA CR-3132.
- Thacker, D.L., C.J. Gibbins, P.R. Schwartz, and R.M. Bevilacqua (1981): Ground-based microwave observations of mesospheric H₂O in January, and September, 1980, Geophys. Res. Lett., 8, 655.
- Thomas, G.E., J.J. Olivero, E.J. Jensen, W. Schroeder, O.B. Toon (1989): Relation between increasing methane and the presence of ice clouds at the mesopause, Nature, 338, 490.
- Tsou, J.J. (1986): Microwave radiometric measurements of mesospheric water vapor: ground-based observations in both solar absorption and atmospheric emission modes, Phd. Thesis, The Pennsylvania State University, University Park, Pennsylvania.
- Twomey, S. (1977): Introduction to the Mathematics of Inversion in Remote Sensing and Indirect Measurements, Elsevier Science Publishing Company, New York, NY.
- U.S. Standard Atmosphere, 1976, U.S. Government Print Office, Washington, D.C.
- Wasson, J.T., and F.T. Kyte (1987): Comment on "On the influx of small comets into the Earth's upper atmosphere II. Interpretations," Geophys. Res. Lett., 14, 779.

Waters, J.W. (1976): Absorption and emission of atmospheric gases, in Methods in Experimental Physics: Volume 12 (Part B), M.L. Meeks Ed., Academic Press, New York, NY.

Waters, J.W., J.J. Gustincic, P.N. Swanson, and A.R. Kerr (1980): Measurement of upper atmospheric water vapor emission at 183 GHz, in Atmospheric Water Vapor, A. Deepak, T.O. Wilkerson, and L.H. Ruhnke, Eds., Academic Press Inc., New York, NY